Third-order transport coefficients for electrons in N2 and CF4: effects of non-conservative collisions, concurrence with diffusion coefficients and contribution to the spatial profile of the swarm

Third-order transport coefficients for electrons in N_2 and CF_4: effects of non-conservative collisions, concurrence with diffusion coefficients and contribution to the spatial profile of the swarm

I Simonović[1], D Bošnjaković[1], Z Lj Petrović[2,3], R D White[4] and S Dujko[1]

[1]Institute of Physics Belgrade, University of Belgrade, Pregrevica 118, 11080 Belgrade, Serbia
[2]University of Ulster, Newtownabbey, Antrim, Northern Ireland, United Kingdom
[3]Serbian Academy of Sciences and Arts, Knez Mihailova 35, 11000 Belgrade, Serbia
[4]College of Science and Engineering, James Cook University, Townsville, QLD 4811, Australia

E-mail: sasha@ipb.ac.rs

September 2021

Abstract. Using a multi-term solution of the Boltzmann equation and Monte Carlo simulation technique we study behaviour of the third-order transport coefficients for electrons in model gases, including the ionisation model of Lucas and Saelee and modified Ness-Robson model of electron attachment, and in real gases, including N_2 and CF_4. We observe negative values in the E/n_0-profiles of the longitudinal and transverse third-order transport coefficients for electrons in CF_4 (where E is the electric field and n_0 is the gas number density). While negative values of the longitudinal third-order transport coefficients are caused by the presence of rapidly increasing cross sections for vibrational excitations of CF_4, the transverse third-order transport coefficient becomes negative over the E/n_0-values after the occurrence of negative differential conductivity. The discrepancy between the two-term approximation and the full multi-term solution of the Boltzmann equation is investigated for electrons in N_2 and CF_4. While the accuracy of the two-term approximation is sufficient to investigate the behaviour of the third-order transport coefficients in N_2, it produces large errors and is not even qualitatively correct for electrons in CF_4. The influence of implicit and explicit effects of electron attachment and ionisation on the third-order transport tensor is investigated. In particular, we discuss the effects of attachment heating and attachment cooling on the third-order transport coefficients for electrons in the modified Ness-Robson model, while the effects of ionisation are studied for electrons in the ionisation model of Lucas and Saelee, N_2 and CF_4. The concurrence between the third-order transport coefficients and the components of the diffusion tensor, and the contribution of the longitudinal component of the third-order transport tensor to the spatial profile of the swarm are also investigated. For electrons in CF_4 and CH_4, we found that the contribution of the component of the third-order transport tensor to the spatial profile of the swarm between approximately 50 Td and 700 Td, is almost identical to the corresponding contribution for electrons in N_2. This suggests that the

recent measurements of third-order transport coefficients for electrons in N_2 may be extended and generalized to other gases, such as CF_4 and CH_4.

Keywords: Third-order transport coefficients, Boltzmann equation, Monte Carlo simulation, electron transport, ionisation, electron attachment

Submitted to: *Plasma Sources Sci. Technol.*

1. Introduction

Non-equilibrium plasmas have a wide range of important applications including micro and nano-electronic device fabrication [1–4], surface etching [5, 6], sputtering [7, 8], chemical processing [9, 10], and plasma medicine [11–13]. The modeling of non-equilibrium plasma is important for further development and optimization of these applications [14–17]. However, this can be quite challenging due to a wide variety of effects that determine the nature of non-equilibrium plasma. These effects include collisions of electrons and ions with neutral particles of the background fluid [18–20], kinetics of excited species [21–23], generation of fast neutrals [24], space charge effects [25,26], and plasma-surface interaction [27,28]. Despite their simplicity, charged-particle swarms are at the heart of non-equilibrium plasma modeling [2, 18, 29, 30]. Specifically, transport coefficients that describe the dynamics of a swarm of charged particles are used as input data into the fluid models of non-equilibrium plasma [31–38]. In addition, transport coefficients are required in the swarm procedure for determining the complete and consistent sets of cross-sections for collisions of charged particles with atoms and molecules of the background fluid [39–42]. These sets of cross-sections are employed as input data into the particle models of non-equilibrium plasma [43–49]. Due to the sensitivity of plasma models to transport coefficients and cross-section sets in the case of fluid and particle models, respectively, a great amount of attention has been dedicated to the calculation and measurement of transport coefficients of electrons and ions in numerous atomic and molecular gases. However, this attention has been limited to the lower-order transport coefficients such as rate coefficients for non-conservative processes, drift velocity, and diffusion tensor components [18, 19, 50].

Transport coefficients of third and higher order have been implemented to analyse ion swarm experiments [51–54]. However, they have been almost systematically ignored in the traditional analysis of electron swarm experiments, as they are difficult to measure and difficult to study by employing theoretical methods [55–57]. However, Kawaguchi and coworkers have recently measured third-order transport coefficients for electrons in molecular nitrogen by employing the arrival time spectra experiment [58]. In addition, they have shown that it is necessary to consider the longitudinal component of the third-order transport tensor Q_L in order to correctly determine the longitudinal component of the diffusion tensor D_L from the arrival time spectra data. The difference between the values of D_L, which are estimated after neglecting Q_L, and the corresponding values,

which are determined from the expression that includes Q_L, is greater than the sum of their experimental errors at high electric fields. Moreover, it is known that the third-order transport coefficients are required for the conversion of hydrodynamic flux transport coefficients into transport parameters that are determined from the steady state Townsend experiment [59]. Third-order transport coefficients are more sensitive to energy dependence of the cross sections for the scattering of charged particles on the constituents of the background medium than drift velocity and diffusion tensor [55,60,61]. For this reason, third-order transport coefficients would be very useful in the swarm procedure for determining the complete sets of cross sections, if these transport coefficients were calculated and measured with a sufficient precision. Kawaguchi *et al.* [58] have shown that the third-order transport coefficients are sensitive to the anisotropy of electron scattering. Thus, inclusion of the third-order transport coefficients would help in testing the implementation of anisotropic scattering in transport calculations, if the values of these transport coefficients were known from experiments [62]. This is important as the correct implementation of anisotropic scattering is required for determining the values of the rate coefficient for electron impact ionisation at high electric fields, with high precision [62, 63].

The structure of the third-order transport tensor in the electric field only configuration was determined by Whealton and Mason [64], Vrhovac *et al.* [55] and Koutselos [52]. Simonović and coworkers have determined the structure of this tensor in all configurations of electric and magnetic field, and they have investigated the physical interpretation of the individual components of this tensor [57]. Koutselos studied the third-order transport coefficients for ions in atomic gases, by employing molecular dynamics simulations and a three-temperature method for solving the Boltzmann equation [52, 65–67]. Third-order transport coefficients for electrons in noble gases were investigated by Penetrante and Bardsley [60], Vrhovac *et al.* [55] and Simonović *et al.* [68]. Penetrante and Bardsley used the two-term approximation for solving the Boltzmann equation and Monte Carlo simulations, Vrhovac *et al.* employed the momentum transfer theory and generalized Einstein relations, while Simonović *et al.* used a multi-term theory for solving the Boltzmann equation. Stokes and coworkers investigated the effects of localized and delocalized electron states on the third-order transport coefficients [69]. Recently, Kawaguchi *et al.* [70] have shown that the third-order transport coefficients can be measured in the arrival time spectra experiment by employing Monte Carlo simulations, and they have determined the values of these transport coefficients for electrons in CH_4 and SF_6 by using the same method. They have subsequently measured the longitudinal component of the third-order transport tensor for electrons in N_2 by employing the arrival time spectra experiment. Kawaguchi *et al.* have further verified these results by using Monte Carlo simulations [58, 62].

Although the lower-order transport coefficients have been carefully investigated in the literature, the third-order transport coefficients are still largely unexplored. For this reason, a number of questions concerning the properties of these transport coefficients and their dependence on elementary scattering processes are still open. How

sensitive are these transport coefficients to effects of non-conservative collisions such as ionisation and electron attachment? Are the differences between the flux and bulk values of the third order transport coefficients higher or lower than the corresponding differences in the lower order transport coefficients? Is there any concurrence between these transport coefficients and those of lower-order? If such concurrence exists, how can it be accounted for? Can third-order transport coefficients be negative, and what would the negative values of these transport coefficients mean physically? Some of these issues will be addressed in this work. Implicit and explicit effects of electron attachment and ionisation on the third-order transport tensor are investigated, for electrons in Ness-Robson model and Lucas-Saelee model, respectively, by employing Monte Carlo simulations and a multi-term method for solving the Boltzmann equation. In addition, explicit effects of ionisation on this transport tensor for electrons in N_2 and CF_4 are studied. Negative values of the third-order transport coefficients for electrons in CF_4 are also investigated. The concurrence between these transport coefficients and diffusion is analysed for electrons in N_2 and CF_4. The values of the longitudinal component of the third-order transport tensor for electrons in N_2, that are determined in this work, are compared with results of Kawaguchi *et al.* The contribution of the third-order transport coefficients to the spatial profile of the swarm is determined for electrons in N_2, CF_4 and CH_4 over a wide range of the reduced electric field. The third-order transport coefficients are defined in section 2. The methods for calculating these transport coefficients by employing a multi-term solution of the Boltzmann equation and Monte Carlo simulations are discussed in sections 3.1 and 3.2, respectively. The cross sections for model and real gases, that are used as input data in this work, are discussed in section 4.1. The variation of the flux third-order transport tensor with the reduced electric field for electrons in N_2 and CF_4 is analysed in section 4.2. The impact of electron attachment on the third-order transport coefficients for electrons in the modified Ness-Robson model is studied in section 4.3.1, while the influence of electron impact ionisation on these transport coefficients for electrons in Lucas-Saelee model, N_2 and CF_4 is investigated in Section 4.3.2. The longitudinal component of the third-order transport tensor, that is determined in this study, is compared with the measurements and calculations of Kawaguchi and coworkers in section 4.4. Concurrence between the third-order transport coefficients and individual components of the diffusion tensor for electrons in N_2 and CF_4 is analysed in this section as well. In the same section the contribution of the third-order transport coefficients to the spatial profile of the swarm is determined for electrons in N_2, CF_4 and CH_4. The concluding remarks are given in section 5.

2. Theory

Transport coefficients are defined for a swarm of charged particles in hydrodynamic conditions. A swarm is an ensemble of charged particles that moves in a neutral background fluid under the influence of an external electric and/or magnetic field. The

density of charged particles is considered to be small, so that their mutual interactions, as well as the effects induced by the space-charge, are neglected. The swarm gains energy from the external electric field and it dissipates this energy input into collisions with the particles of the background fluid. However, the probability of having collisions with molecules perturbed/excited by the swarm itself is negligible due to a low swarm particle density.

If the external fields are uniform in space, the swarm relaxes to a stationary state in which the amount of energy that is gained per unit time, is equal to the amount of energy that is dissipated in collisions during this time. The influence of the swarm on the background fluid and fields is neglected, due to the low density of charged particles, and it is considered that this fluid is in a state of thermodynamic equilibrium. Hydrodynamic conditions are fulfilled for a swarm of charged particles if the background fluid and the electric/magnetic fields are spatially homogeneous, and if the swarm is far from the boundaries of the system and far from sources and sinks of charged particles. Under these conditions the phase space distribution function can be expanded into a density gradient series as [71]:

$$f(\mathbf{r},\mathbf{c},t)=\sum_{k=0}^{\infty}\mathbf{f}^{(k)}(\mathbf{c})\odot(-\nabla)^k n(\mathbf{r},t), \tag{1}$$

where $\mathbf{r}$, $\mathbf{c}$ and t are radius vector, velocity vector and time, respectively, $\mathbf{f}^{(k)}(\mathbf{c})$ are tensors of rank k, $\odot$ is tensor contraction of order k, while $n(\mathbf{r},t)$ is number density of charged particles. Under hydrodynamic conditions the flux of velocity of charged particles can be written as [55]:

$$\mathbf{\Gamma}(\mathbf{r},t)=\mathbf{W}^{(f)}n(\mathbf{r},t)-\hat{\mathbf{D}}^{(f)}\cdot\nabla n(\mathbf{r},t)+\hat{\mathbf{Q}}^{(f)}\odot(\nabla\otimes\nabla)n(\mathbf{r},t)+..., \tag{2}$$

where $\mathbf{W}^{(f)}$, $\hat{\mathbf{D}}^{(f)}$ and $\hat{\mathbf{Q}}^{(f)}$ are flux drift velocity, flux diffusion tensor and flux third-order transport tensor, respectively, and $\otimes$ is the tensor product. The equation (2) is truncated at the third term, as this is sufficient for defining the flux third-order transport tensor. Explicit expressions for the flux transport coefficients in terms of the phase space distribution function are given in reference [57].

Bulk transport coefficients appear in the generalized diffusion equation [55], which has been truncated at the third-order gradients for our needs:

$$\begin{aligned}\frac{\partial n(\mathbf{r},t)}{\partial t}&+\mathbf{W}^{(b)}\cdot\nabla n(\mathbf{r},t)-\hat{\mathbf{D}}^{(b)}:(\nabla\otimes\nabla)n(\mathbf{r},t)\\&+\hat{\mathbf{Q}}^{(b)}\vdots(\nabla\otimes\nabla\otimes\nabla)n(\mathbf{r},t)=R_i n(\mathbf{r},t),\end{aligned} \tag{3}$$

where $\mathbf{W}^{(b)}$, $\hat{\mathbf{D}}^{(b)}$, $\hat{\mathbf{Q}}^{(b)}$ and R_i are bulk drift velocity, bulk diffusion tensor, bulk third-order transport tensor and effective rate coefficient for non-conservative processes, respectively, while : and $\vdots$ represent tensor contractions of second and third-order, respectively. Bulk transport coefficients can be expressed in terms of flux transport coefficients as [57]:

$$\mathbf{W}^{(b)}=\mathbf{W}^{(f)}+\mathbf{S}^{(1)},\ \ \hat{\mathbf{D}}^{(b)}=\hat{\mathbf{D}}^{(f)}+\mathbf{S}^{(2)},\ \ \hat{\mathbf{Q}}^{(b)}=\hat{\mathbf{Q}}^{(f)}+\mathbf{S}^{(3)} \tag{4}$$

where $\mathbf{S}^{(k)}$ is the coefficient in the hydrodynamic expansion of the source term, that is contracted with k-th derivative of the density gradient. For a swarm of electrons in the presence of electron impact ionisation and/or electron attachment, the source term is defined as:

$$S(\mathbf{r},t) = \int n_0 c\Big(\sigma_i(\epsilon) - \sigma_a(\epsilon)\Big) f(\mathbf{r},\mathbf{c},t) d\mathbf{c}, \tag{5}$$

where n_0, ϵ, $\sigma_i(\epsilon)$ and $\sigma_a(\epsilon)$ are number density of the background molecules, electron energy, and cross sections for ionisation and electron attachment, respectively.

Implicit effects of non-conservative collisions arise due to population and depopulation of different parts of the distribution function in velocity space, that are caused by the energy dependence of collision frequencies of non-conservative processes. These effects refer to the influence of non-conservative collisions on tensors $\mathbf{f}^{(k)}(\mathbf{c})$ in equation (1). Explicit effects of non-conservative processes arise due to the spatial dependence of collision frequencies for these processes. This spatial dependence is caused by the energy dependence of the collision frequencies for non-conservative collisions and spatial variation of energy of charged particles. Explicit effects of non-conservative collisions are represented by tensors $\mathbf{S}^{(k)}$ from the equation (4) and they determine the difference between flux and bulk transport coefficients.

The influence of implicit and explicit effects of non-conservative collisions on low order transport coefficients has been thoroughly studied in previous publications [72,74]. Implicit effects of ionisation on the third-order transport coefficients refer to the influence of ionisation cooling on the asymmetric component of the diffusive flux, which is represented by the flux third-order transport tensor. Due to explicit effects of ionisation more electrons are created at the front of the swarm than at the back of the swarm, which in turn elongate the spatial distribution of electrons along both longitudinal and transverse directions at the leading edge of the swarm. Similarly, the implicit effects of electron attachment relate to the influence of depopulation of low-energy part of the distribution function, in case of attachment heating, and depopulation of high-energy part of the distribution function, in case of attachment cooling, on the asymmetric component of the diffusive flux. Explicit effects of electron attachment on the third-order transport coefficients refer to the influence of the spatial variation of electron losses to the compression of the spatial distribution of the swarm in those regions of space where electron attachment is more frequent.

The studied system is a swarm of electrons which move in a homogeneous background gas under the influence of a homogeneous and constant electric field that is oriented along the z axis. In this field configuration the flux third-order transport tensor has three independent components Q_{zzz}, Q_{xxz} and Q_{zxx}. In this field configuration, the following relations are imposed on the off-diagonal components of the flux third-order transport tensor: $Q_{xxz} = Q_{xzx} = Q_{yyz} = Q_{yzy}$ and $Q_{zxx} = Q_{zyy}$ [52, 55, 57, 64]. The structure of the third-order transport tensor and physical interpretation of its individual components are extensively discussed in our recent work [57]. In particular, contribution of the third-order transport coefficients to the spatial profile of the swarm is represented

by the following approximate expression [57]:

$$n^{(1)}\left(\mathbf{r},t\right)=n^{(0)}\left(\mathbf{r},t\right)\left[1+\frac{tQ_L^{(b)}}{\sigma_z^3}\chi_z\Big(\chi_z^2-3\Big)+\frac{3tQ_T^{(b)}}{\sigma_x^2\sigma_z}\chi_z\Big(\chi_x^2+\chi_y^2-2\Big)\right], \quad (6)$$

where $n^{(0)}(\mathbf{r},t)$ is the solution of the diffusion equation in which third and higher order transport coefficients are neglected, $Q_L=Q_{zzz}$, $Q_T=\frac{1}{3}(Q_{xxz}+Q_{xzx}+Q_{zxx})$, $\sigma_z=\sqrt{2D_L^{(b)}t}$ and $\sigma_x=\sigma_y=\sqrt{2D_T^{(b)}t}$, while χ_z, χ_x, χ_y are defined as:

$$\chi_z=\frac{z-W^{(b)}t}{\sigma_z},\quad \chi_x=\frac{x}{\sigma_x},\quad \chi_y=\frac{y}{\sigma_y}. \quad (7)$$

The equation (6) can be derived from the Fourier transform of the generalized diffusion equation in which third-order transport coefficients are included [57]. It can be seen from equation (6) that contribution of the longitudinal component of the third-order transport tensor to the spatial profile of the swarm is proportional to $Q_L^{(b)}/(D_L^{(b)})^{3/2}$. In statistics the asymmetry of the probability distribution of a random variable about its expected value is represented by skewness [73]. There are several ways to express skewness in statistics including the third central moment and the third standardized moment of a random variable [73]. It can be shown that the bulk third-order transport tensor is proportional to the third central moment of the position vector, while $Q_L^{(b)}/(D_L^{(b)})^{3/2}$ is proportional to the longitudinal component of the third standardized moment of the position vector. Likewise, the $Q_T^{(b)}/(D_T^{(b)}(D_L^{(b)})^{1/2})$ term is proportional to the off-diagonal component of the same standardized moment with the combination of indices π_{xxz}, where π_{abc} represents any permutation of a, b and c.

The flux third-order transport tensor is defined by the flux gradient relation. The last two indices of this tensor are contracted with partial derivatives of the charged-particle number density with respect to spatial coordinates. The third-order bulk transport tensor is however defined by the generalised diffusion equation, in which the three indices of this tensor are contracted with partial derivatives. For this reason, all three indices of the bulk third-order transport tensor commute, as this transport property is symmetrized in the equation in which it is defined. The same reasoning applies to the bulk diffusion tensor and higher order bulk transport tensors. Using these arguments, in the case of bulk third-order transport coefficients and when the swarm of charged-particles is acted on solely by an electric field, we can identify only two independent bulk components $Q_L^{(b)}$ and $Q_T^{(b)}$. In a more general configuration of electric and magnetic fields, we can identify those components of the bulk third-order transport tensor that are symmetrized along all three indices. These are third-order transport coefficients that can be distinguished in our Monte Carlo simulations, as we calculate transport coefficients using expressions derived from the generalized diffusion equation [57].

3. Methodology

3.1. Multi-term solution of the Boltzmann equation

The Boltzmann equation describes the evolution of the phase space distribution function $f(\mathbf{r}, \mathbf{c}, t)$. For a swarm of electrons the Boltzmann equation can be written as:

$$\frac{\partial f(\mathbf{r}, \mathbf{c}, t)}{\partial t} + \mathbf{c} \cdot \frac{\partial f(\mathbf{r}, \mathbf{c}, t)}{\partial \mathbf{r}} + \frac{q}{m}\mathbf{E} \cdot \frac{\partial f(\mathbf{r}, \mathbf{c}, t)}{\partial \mathbf{c}} = -J(f, f_0), \tag{8}$$

where q and m are electron charge and electron mass respectively, $\mathbf{E}$ is electric field and J is collision operator. This operator represents change of the electron distribution function per unit time, due to collisions with particles of the background medium. These particles are described by the distribution function f_0.

In the multi-term method for solving Boltzmann's equation the phase space distribution function is expanded in terms of spherical harmonics and Sonine polynomials in angular and radial parts of the velocity space, respectively. Thus, under hydrodynamic conditions $f(\mathbf{r}, \mathbf{c}, t)$ is expanded as follows [74–78]:

$$f(\mathbf{r}, \mathbf{c}, t) = \omega(\alpha, c) \sum_{s=0}^{\infty} \sum_{\lambda=0}^{s} \sum_{\mu=-\lambda}^{\lambda} \sum_{\nu,l=0}^{\infty} \sum_{m=-l}^{l} F(\nu l m | s\lambda\mu; \alpha) R_{\nu l}(\alpha, c) Y_m^{[l]}(\hat{\mathbf{c}}) G_\mu^{(s\lambda)} n(\mathbf{r}, t) \tag{9}$$

where $F(\nu l m | s\lambda\mu; \alpha)$ are moments of the distribution function, $\hat{\mathbf{c}}$ is unit vector in velocity space, $Y_m^{[l]}(\hat{\mathbf{c}})$ are spherical harmonics, $G_\mu^{(s\lambda)}$ is the spherical form of the gradient tensor operator, while α, $\omega(\alpha, c)$ and $R_{\nu l}(\alpha, c)$ are given by:

$$\alpha^2 = \frac{m}{kT_b}, \tag{10}$$

$$\omega(\alpha, c) = \left(\frac{\alpha^2}{2\pi}\right)^{3/2} e^{-\alpha^2 c^2/2}, \tag{11}$$

$$R_{\nu l}(\alpha c) = N_{\nu l} \left(\frac{\alpha c}{\sqrt{2}}\right)^2 S_{l+1/2}^{(\nu)}(\alpha^2 c^2/2), \tag{12}$$

where k is the Boltzmann constant, T_b is the basis temperature, which is a parameter for optimizing convergence, $S_{l+1/2}^{(\nu)}$ is Sonine polynomial, while $N_{\nu l}$ is given by:

$$N_{\nu l}^2 = \frac{2\pi^{3/2}\nu!}{\Gamma(\nu + l + 3/2)}, \tag{13}$$

where $\Gamma(\nu + l + 3/2)$ is gamma function.

The Boltzmann equation is decomposed into a hierarchy of kinetic equations by applying the relations of orthogonality for spherical harmonics and Sonnine polynomials [75]. The moments of the distribution function $F(\nu l m | s\lambda\mu; \alpha)$ can be obtained by solving this system of kinetic equations [74, 79]. The resulting hierarchy of kinetic equations is truncated at finite values of $l = l_{max}$ and $\nu = \nu_{max}$. Unlike the two-term approximation, in which small anisotropy in velocity space is assumed and l_{max} is set to 1, in the multi-term method l_{max} is increased until full convergence of transport coefficients is obtained, after which the obtained hierarchy is solved numerically.

Spherical form of the velocity vector is defined as [75]:

$$c_m^{[1]} = \sqrt{\frac{4\pi}{3}} c Y_m^{[1]}(\hat{\mathbf{c}}). \tag{14}$$

Cartesian components of a vector can be expressed via spherical form as:

$$c_x = \frac{i}{\sqrt{2}}\left(c_1^{[1]} - c_{-1}^{[1]}\right), \tag{15}$$

$$c_y = \frac{1}{\sqrt{2}}\left(c_1^{[1]} + c_{-1}^{[1]}\right), \tag{16}$$

$$c_z = -i c_0^{[1]}. \tag{17}$$

Spherical form of the flux of velocity of electrons can be written as [79]:

$$\Gamma_m^{(1)}(\mathbf{r}, t) = \frac{1}{\alpha} \sum_{s=0}^{\infty} \sum_{\lambda=0}^{s} \sum_{\mu=-\lambda}^{\lambda} F(01m|s\lambda\mu)\, G_\mu^{(s\lambda)} n(\mathbf{r}, t)\,. \tag{18}$$

Explicit expressions for the individual components of the flux third-order transport tensor can be determined from the Cartesian components of the flux of velocity from equation (18) after identifying terms that are contracted with the corresponding partial derivatives [57].

Expressions for three independent components of the flux third-order transport tensor in the electric field only configuration defined to be in the z direction, are given by:

$$Q_{xxz}^{(f)} = \frac{1}{\sqrt{2}\alpha}\left[\mathrm{Im}(F(011|221;\alpha)) - \mathrm{Im}(F(01-1|221;\alpha))\right], \tag{19}$$

$$\begin{aligned} Q_{zxx}^{(f)} = & -\frac{1}{\alpha}\left[\frac{1}{\sqrt{3}}\mathrm{Im}(F(010|200;\alpha)) + \frac{1}{\sqrt{6}}\mathrm{Im}(F(010|220;\alpha))\right] \\ & + \frac{1}{\alpha}\mathrm{Im}\left[F(010|222;\alpha)\right], \end{aligned} \tag{20}$$

$$Q_{zzz}^{(f)} = \frac{1}{\alpha}\left[\sqrt{\frac{2}{3}}\mathrm{Im}(F(010|220;\alpha)) - \frac{1}{\sqrt{3}}\mathrm{Im}(F(010|200;\alpha))\right], \tag{21}$$

where Im denotes imaginary parts of the moments of the phase space distribution function.

3.2. Monte Carlo simulations

In Monte Carlo simulations, we track the space and time evolution of a swarm of electrons. The extensive use of random numbers is required in order to determine the exact moment and the type of the individual collisions of electrons with the background molecules, as well as the direction of the post collisional electron velocity. The transport coefficients are computed from the corresponding polynomials of the electron coordinates and velocity components, which are averaged over the entire swarm. The details of our

Monte Carlo code are discussed in our previous publications [74,80–82]. Bulk third-order transport coefficients are calculated as:

$$\mathbf{Q}^{(b)} = \frac{1}{3!}\frac{\mathrm{d}}{\mathrm{d}t}\langle \mathbf{r}^\star \mathbf{r}^\star \mathbf{r}^\star \rangle, \tag{22}$$

while the flux third-order transport coefficients are determined from:

$$\mathbf{Q}^{(f)} = \frac{1}{3!}\left\langle \frac{\mathrm{d}}{\mathrm{d}t}\Big(\mathbf{r}^\star \mathbf{r}^\star \mathbf{r}^\star\Big) \right\rangle, \tag{23}$$

where $\mathbf{r}^\star = \mathbf{r} - \langle \mathbf{r} \rangle$, and the brackets $\langle\rangle$ represent ensamble averages. Expressions for transport coefficients, that are used in our Monte Carlo method, are derived from the generalized diffusion equation, in which all tensor indices are contracted with partial derivatives. Thus, in the generalized diffusion equation symmetrization of the third-order transport tensor with respect to all indices is performed. For this reason, we cannot determine individual off-diagonal components of the third-order transport tensor or individual off-diagonal components of the diffusion tensor in our Monte Carlo simulations [74]. Instead, we can determine individual diagonal components such as $Q_L = Q_{zzz}$ and averages of those off-diagonal components that have the same combination of indices like $Q_T = (Q_{xxz} + Q_{xzx} + Q_{zxx})/3$. It should be noted that Q_{xxz} and Q_{xzx} are equal due to the commutativity of the last two indices of the third-order transport tensor [52,55,57,64]. Explicit expressions for $Q_L^{(b)}$ and $Q_T^{(b)}$ in the electric field only configuration are given by:

$$Q_L^{(b)} = \frac{1}{6}\frac{\mathrm{d}}{\mathrm{d}t}\Big(\langle z^3 \rangle - 3\langle z \rangle \langle z^2 \rangle + 2\langle z \rangle^3\Big), \tag{24}$$

$$Q_T^{(b)} = \frac{1}{6}\frac{\mathrm{d}}{\mathrm{d}t}\Big(\langle z x^2 \rangle - \langle z \rangle \langle x^2 \rangle\Big), \tag{25}$$

while the corresponding flux components $Q_L^{(f)}$ and $Q_T^{(f)}$ are given in [57].

It is important to note that numerical differentiation in time is not used for the calculation of $Q_L^{(b)}$ and $Q_T^{(b)}$, because of the statistical fluctuations of the corresponding expressions in brackets. Direct numerical differentiation of these expressions would create fluctuations that are much more intense than the fluctuations of the initial expressions. Instead, the expression in brackets is fitted to a linear function. The corresponding time derivative is determined as the slope of this linear function. This is justified because $Q_L^{(b)}$ and $Q_T^{(b)}$ are independent of time after relaxation of the swarm, and the corresponding expressions in brackets in equations (24) and (25) are linear functions in time. This method for calculating $Q_L^{(b)}$ and $Q_T^{(b)}$ has been further verified by comparing values of the bulk third-order transport coefficients, that are obtained by this method, with the corresponding values that are determined by employing numerical differentiation in time. An additional check was obtained by comparing $Q_L^{(b)}$ and $Q_T^{(b)}$ with $Q_L^{(f)}$ and $Q_T^{(f)}$, respectively, under conditions where non-conservative processes are absent.

4. Results and discussion

4.1. Preliminaries

In this paper, we consider the transport of electrons in the Lucas-Saelee model, modified Ness-Robson model, N_2 and CF_4. The Ness-Robson model was developed for testing the multi-term method for solving the Boltzmann equation in the presence of electron attachment [79]. Nolan and coworkers presented a new gas model that is based on the Ness-Robson model and the Lucas-Saelee model [72]. In this model the collision frequency of elastic collisions is independent of energy while the cross section for inelastic collisions is the same as in the Lucas-Saeele model. In modifying the Ness-Robson model, which is introduced by Nolan *et al.* [72], both inelastic collisions and ionisation are present. The ratio of the cross section for inelastic collisions to the cross section for ionisation is determined by the F parameter, as in the Lucas-Saelee model. Two different versions of the modified Ness-Robson model [72] with different functional dependences of the cross section for electron attachment are considered in this work. In both considered versions of the modified Ness-Robson model the parameter F is set to zero, implying the absence of ionisation. The details of the modified Ness-Robson model, in the absence of ionisation, are given by the following equations:

$$\begin{aligned}
&\sigma_{el}(\epsilon) = 4\epsilon^{-1/2}\text{Å}^2 \ \text{(elastic collision)}\\
&\sigma_{ex}(\epsilon) = \begin{cases} 0.1(\epsilon - 15.6)\ \text{Å}^2, & \epsilon \geq 15.6\ \text{eV} \\ & \text{(inelastic collision)} \\ 0, & \epsilon < 15.6\text{eV} \end{cases}\\
&\sigma_a(\epsilon) = a\epsilon^p \ \text{(electron attachment)}\\
&m/m_0 = 10^{-3},\\
&T_0 = 0\ \text{K}\,,
\end{aligned} \tag{26}$$

where $\sigma_{el}(\epsilon)$, $\sigma_{ex}(\epsilon)$, $\sigma_a(\epsilon)$ are cross sections for elastic collisions, inelastic collisions and electron attachment, respectively, given as functions of electron energy ϵ, T_0 is the temperature of the background gas, while m and m_0 are masses of electrons and of the molecules of the background gas, respectively. In the above equations, the values of the electron energy are given in eV. Parameters a and p determine the magnitude and the functional dependence of the cross section for electron attachment, respectively. The values of p that are considered in this work include -1.0 and 0.5. These values correspond to attachment heating and attachment cooling, respectively. The percentage differences between the third-order transport coefficients determined for each of these two models and the corresponding values in the model where $p = -0.5$ are considered in this work. In the third model the collision frequency for electron attachment is independent of energy. The values of parameter a, that are used in this work, include $8 \cdot 10^{-3}\text{Å}^2$ and $5 \cdot 10^{-4}\text{Å}^2$. The first value is used for the attachment heating model, while the second value is used for the attachment cooling model. In the model with constant collision frequency for electron attachment, this non-conservative process is

equally frequent at all values of the electron energy, and it does not affect transport coefficients of any order (excluding the rate coefficient for electron attachment). In this model the values of the third-order transport tensor are the same as in the conservative Lucas-Saelee model, where $F = 0$.

The Lucas-Saelee ionisation model was introduced in order to investigate the influence of electron-impact ionisation on the electron transport by using Monte Carlo simulations [83]. Ness and Robson investigated the electron transport in this model, in order to test the validity of the theory and associated computer code for solving the Boltzmann equation, in the presence of non-conservative processes [79]. The details of the Lucas-Saelee model are given by the following equations:

$$\begin{aligned}
&\sigma_{el}(\epsilon) = 4\epsilon^{-1/2}\text{Å}^2 \ \text{(elastic collision)} \\
&\sigma_{ex}(\epsilon) = \begin{cases} 0.1(1-F)(\epsilon - 15.6)\ \text{Å}^2, & \epsilon \geq 15.6\ \text{eV} \\ & \text{(inelastic collision)} \\ 0, & \epsilon < 15.6\text{eV} \end{cases} \\
&\sigma_I(\epsilon) = \begin{cases} 0.1F(\epsilon - 15.6)\ \text{Å}^2, & \epsilon \geq 15.6\ \text{eV} \\ & \text{(ionisation)} \\ 0, & \epsilon < 15.6\text{eV} \end{cases} \\
&P(q, \epsilon') = 1, m/m_0 = 10^{-3}, \\
&T_0 = 0\ \text{K}\,,
\end{aligned} \tag{27}$$

where $\sigma_I(\epsilon)$ is the cross section for ionisation, $P(q, \epsilon)$ is the ionisation partition function, and F is the parameter that determines the magnitudes of cross sections for inelastic collisions and ionisation. As the scattering is isotropic in this model $\sigma_{el}(\epsilon)$, $\sigma_{ex}(\epsilon)$, and $\sigma_I(\epsilon)$ represent total cross sections. Arguments of the ionisation partition function $P(q, \epsilon')$, q and ϵ', are the ratio of total postcollisional energy, that is given to the ejected electron, and the energy of the initial electron before ionisation, respectively. In this model, ionisation partition function is set to unity, indicating that all values $0 \leq q \leq 1$ are equally probable.

The set of cross sections for electron scattering in N_2, which is used in this work, is detailed in [63]. It includes elastic momentum transfer cross section, as well as the total cross section for rotational excitations, and cross sections for vibrational excitations, electronic excitations and electron-impact ionisation. The set of cross sections for electron scattering in CF_4, which is employed in this work, was developed and discussed by Kurihara and coworkers [84]. It includes elastic momentum transfer cross section, cross sections for vibrational excitations, electronic excitations, electron attachment, and ionisation. For some aspects of this work, it was necessary to consider the electron transport in CH_4. These results are obtained by using the cross sections developed by Šašić *et al.* [85].

The results for the model and the real gases were obtained from the Monte Carlo simulations and numerical multi-term solution of the Boltzmann equation. In particular, it was necessary to follow a large number of electrons (at least 10^7) in our Monte Carlo

simulations in order to calculate third-order transport coefficients accurately, due to high statistical fluctuations of individual terms appearing in expressions (24) and (25). It was also necessary to determine the phase space distribution function with a high degree of precision in order to calculate the third-order transport coefficients from the multi-term method. While the number of spherical harmonics indicates the degree of anisotropy of the phase space distribution function in velocity space, the number of Sonine polynomials is indicative of the deviation of the energy dependence of the distribution function from a Maxwellian at a particular temperature T_b not necessarily equal to the gas temperature T_0. Third-order transport coefficients are more sensitive to the shape of the phase space distribution function than transport coefficients of lower order. For this reason it was necessary to include a large number of spherical harmonics and Sonine polynomials to achieve the convergence of the third-order transport coefficients, in the presence of strong inelastic and/or non-conservative collisions. For example, the required numbers of l_{max} and ν_{max} were 8 and 90, respectively, for electrons in CF_4. This was especially pronounced in the energy region where the cross sections for vibrational excitations are rapidly rising functions of electron energy, while the cross section for elastic collisions is being reduced with increasing electron energy. The solutions of the Boltzmann equation are not determined for $E/n_0 > 300$ Td, as the convergence of the transport coefficients was poor in this field region. For this reason, we have only displayed the Monte Carlo results in the field range above 300 Td.

4.2. Variation of the flux third-order transport coefficients with E/n_0 for electrons in N_2 and CF_4

In figure 1 (a) and 1 (b) we show the mean energy for an electron swarm in N_2, and CF_4, respectively, as a function of the reduced electric field, E/n_0. At the lowest fields the mean energy is thermal in both gases, while it is rising with increasing E/n_0 at higher fields. The slope of the mean energy is determined by collisions of electrons with atoms/molecules of the background gas [84]. The profiles of the mean energy are useful for analysing the field dependence of the third-order transport coefficients. From these profiles one can determine which collisional processes dominate electron transport in a given field range.

In this section, we study the behaviour of the components of the flux third-order transport tensor for electrons in N_2 and CF_4 in the presence of an electric field. It has been previously shown that the rise of E/n_0 under constant collision frequency conditions leads to an increase of the components of the third-order transport coefficient tensor [57]. It has also been shown that the increase of the collision frequency with increasing energy may lead to a decrease of the components of this tensor, as well as to negative values of these components, if the rise of the collision frequency is steep enough [57,68]. For this reason, the E/n_0-profile of the third-order transport coefficients is determined by the complex interplay between the electric field, which accelerates electrons and acts to direct their movement along the field lines, and collisions between

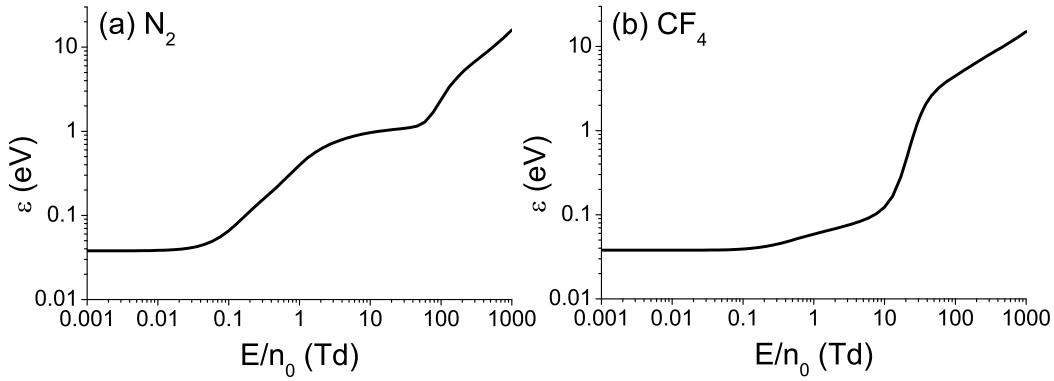

Figure 1. Mean energy of electron swarm in (a) N_2 and (b) CF_4, as a function of the reduced electric field. These results are obtained by using multi term theory for solving the Boltzmann equation up to about 300 Td and by employing Monte Carlo simulations at higher fields.

electrons and atoms/molecules of the background gas, which dissipate electron energy and momentum. Although it is possible to analyse E/n_0 profiles of the third-order transport coefficients directly from the mean energy of electrons and collision frequencies for individual collisional processes, such analysis is often quite complicated and tedious. Therefore, in this section we briefly discuss the general E/n_0-profiles of the third-order transport coefficients for electrons in N_2 and CF_4, while a more detailed analysis is reserved only for the unusual and unexpected aspects of the behaviour of these transport properties. A more detailed study of the behaviour of $Q^{(f)}_{zzz}$ and $Q^{(f)}_T$ for electrons in N_2 and CF_4 is presented in section 4.4.

In figure 2 we show the independent components of the third-order flux transport tensor for electrons in N_2 as functions of E/n_0. In addition, we also show the variation of $n_0^2 Q^{(f)}_T$ with E/n_0. The $Q^{(f)}_{zxx}$ component is negative, while the remaining quantities are positive over the entire E/n_0 range considered. Negative values of $Q^{(f)}_{zxx}$ can be attributed to the rise of the collision frequency for elastic and inelastic collisions with increasing electron energy. This phenomenon has been observed for electrons in both model and real gases [57, 61, 68]. It can be seen from figure 2 that the absolute values of quantities have a similar qualitative dependance on E/n_0. Specifically, the absolute values of these transport coefficients have two local maximums at about 1.3 Td and 150 Td, and a local minimum at around 46 Td.

In figure 3 we show the three independent components of the flux third-order transport tensor for electrons in CF_4 as functions of E/n_0. In the same figure we show the variation of $n_0^2 Q^{(f)}_T$ with E/n_0. At the lowest fields, all quantities are positive, and increasing functions E/n_0 up to about 0.14 Td in the case of $Q^{(f)}_{zzz}$, and up to about 0.18 Td in the case of the remaining quantities. At higher fields these quantities are being reduced and they become negative. The $Q^{(f)}_{zxx}$ component becomes negative at about 2 Td. The remaining transport coefficients become negative at about 0.9 Td, and they reach a local minimum at around 1.6 Td. These quantities become positive

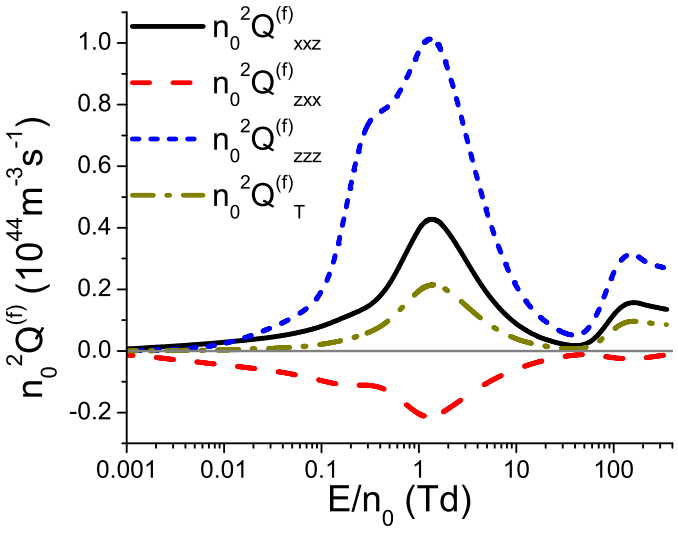

Figure 2. Independent components of the flux third-order transport tensor and $n_0^2 Q_T^{(f)}$ as functions of E/n_0 for electrons in N_2. The results are obtained from numerical multi-term solutions of the Boltzmann equation.

again at about 7.5 Td. The $Q_{xxz}^{(f)}$ and $Q_{zzz}^{(f)}$ components remain positive until the end of the considered range of E/n_0, while the $Q_{zxx}^{(f)}$ component remains negative. The $Q_{zzz}^{(f)}$ component has two local maximums at about 20 Td and 170 Td and a local minimum at around 27 Td. The $Q_{xxz}^{(f)}$ component and $Q_T^{(f)}$ have a local maximum at about 31 Td and 25 Td, and a local minimum at around 120 Td and 100 Td, respectively. The $Q_{zxx}^{(f)}$ component has a local minimum at about 33 Td. At the lowest E/n_0, all quantities that are displayed in figure 3 are rising functions of E/n_0. This can be attributed to a negligible rise of the mean energy with increasing field in this E/n_0 region, which leads to a small change of the mean collision frequency for elastic and inelastic collisions. At higher fields, the rise of the mean energy and mean collision frequency for vibrational excitations with increasing E/n_0, become more significant, which in turn induces a decrease of the third-order transport coefficients.

We now focus on the negative values of the third-order transport coefficients for electrons in CF_4. As discussed elsewhere [57, 69], the bulk third-order transport tensor represents asymmetric deviation of the spatial distribution of the swarm from an ideal Gaussian. This deviation is caused by different rates of spread of electrons at the swarm front and at the back of the swarm. Due to this difference, different parts of the normalized spatial distribution of electrons may seem elongated or compressed when compared to an ideal Gaussian. Specifically, $Q_{zzz}^{(b)}$ component describes elongation/contraction of the spatial distribution of electrons at the leading edge of the swarm, and the opposite deformation at its trailing edge. A negative value of the $Q_{zzz}^{(b)}$ component implies that the normalized spatial distribution of electrons is compressed (when compared to an ideal Gaussian) along the longitudinal direction at the front of the swarm and expanded along the same direction at the back of the swarm. Similarly, a negative value of $Q_T^{(b)}$ implies that the normalized spatial distribution of electrons is

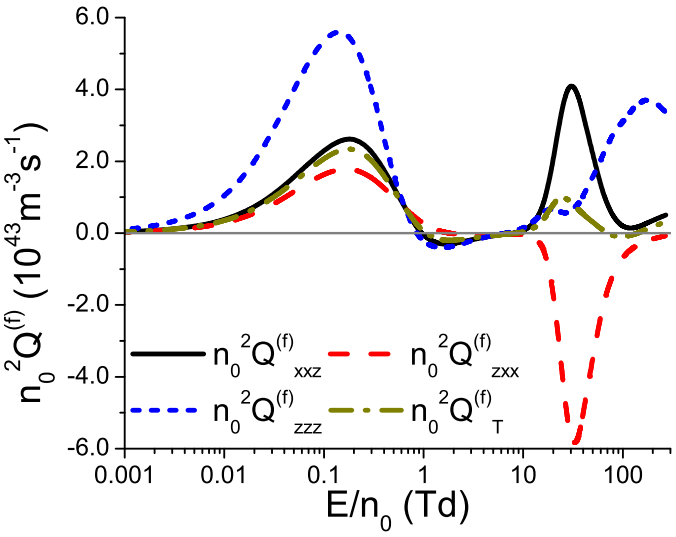

Figure 3. Independent components of the third-order transport tensor and $n_0^2 Q_T^{(f)}$ as functions of E/n_0 for electrons in CF_4. The results are obtained from numerical multi-term solutions of the Boltzmann equation.

compressed (relative to an ideal Gaussian) along the transverse direction at the swarm front and expanded along the same direction at the back of the swarm. It is important to emphasize that the spatial distribution of electrons is not being actually compressed in time. Instead, in some regions of space the effective rate of spread of electrons, that is represented by both third-order transport coefficients and diffusion, is smaller than the corresponding rate of spread that would be represented by diffusion alone. In these regions of space, the normalized spatial distribution of electrons seems compressed when compared to an ideal Gaussian. For E/n_0 less than approximately 10 Td, the impact of non-conservative collisions is minimal, and thereby the bulk values of the third-order transport coefficients are equal to the corresponding flux values (see figure 13). In the field region around 0.9 Td, where $Q_{zzz}^{(f)}$, $Q_{xxz}^{(f)}$ and $Q_T^{(f)}$ become negative, electrons with energies that are 3 times higher than the mean energy are in the energy region around 0.2 eV, where the cross sections for two vibrational excitations of the CF_4 molecule reach their global maximums [84]. These cross sections are denoted as Q_{v1} and Q_{v3} in Table 1 or reference [84] and their thresholds are 0.108 eV and 0.168 eV, respectively. Moreover, Q_{v1} overestimates the elastic momentum transfer cross section in the energy range between approximately 0.12 eV and 0.58 eV. The same holds for Q_{v3} in the energy range between approximately 0.17 eV and 2.6 eV. Thus, in the field region around 0.9 Td where $Q_{xxz}^{(f)}$, $Q_{zzz}^{(f)}$ and $Q_T^{(f)}$ become negative, the high energy tail of the distribution function is in the energy range where the electron transport is dominated by vibrational excitations. As the mean energy of electrons is increasing in the positive direction (direction of the force acting upon electrons), the intense energy losses due to the vibration excitations create a strong resistance to the spreading of the swarm at its front in the longitudinal and transverse directions. This resistance leads to the

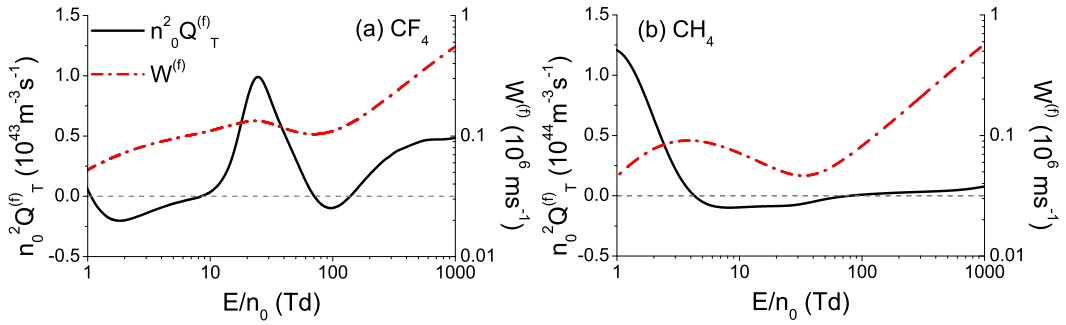

Figure 4. Transverse flux third-order transport coefficients $n_0^2 Q_T^{(f)}$ and the flux drift velocity $W^{(f)}$ as functions of E/n_0 for electrons in (a) CF_4 and (b) CH_4. The results are obtained by employing the multi-term theory for solving the Boltzmann equation up to about 300 Td for electrons in CF_4, and up to 600 Td for electrons in CH_4, and by using Monte Carlo simulations at higher fields.

compression of the spatial distribution of electrons at the front of the swarm along both longitudinal and transverse directions, while this spatial distribution is more expanded along both these directions at the back of the swarm. Such deviation of the spatial profile of electrons from an ideal Gaussian is manifested through negative values of Q_{zzz} and Q_T (in both flux and bulk case).

In figures 4 (a) and (b), we show the variation of $n_0^2 Q_T^{(f)}$ and $W^{(f)}$ with E/n_0 for electrons in CF_4 and CH_4, respectively. It should be noted that some general aspects of the behaviour of third-order transport coefficients for electrons in CH_4 were discussed in our previous publication [61]. CH_4 was introduced here in order to observe relationship of negative values of the higher order transport coefficients with the negative differential conductivity (NDC) for drift velocity. We observe from figures 4 (a) and (b) that the drift velocity of electrons in both CF_4 and CH_4 exhibits NDC. NDC refers to the decrease in drift velocity with an increase in the reduced electric field E/n_0. To understand NDC, it is necessary to consider the rates of momentum and energy transfer in elastic and inelastic collisions [86]. Interestingly, Q_T has negative values between approximately 70 Td and 140 Td in CF_4. This approximately corresponds to the field region beyond the end of the NDC where drift velocity begins to rise rapidly (almost reaching its maxmum value before the NDC). A similar relationship exists in the E/n_0-profile of the electron drift velocity in CH_4. However, in CH_4, Q_T becomes negative at the beginning of the NDC much earlier than in CF_4.

The qualitative behaviour of the individual off-diagonal components of the third-order transport tensor over the range of E/n_0, where NDC occurs, is different for electrons in CF_4 and CH_4. For electrons in CF_4 the $Q_{xxz}^{(f)}$ component is positive, while the $Q_{zxx}^{(f)}$ component is negative, over the entire range of E/n_0, corresponding to the NDC. For the electrons in CH_4, however, the $Q_{xxz}^{(f)}$ component becomes negative shortly after the start of the NDC, while $Q_{zxx}^{(f)}$ becomes positive at a slightly larger field. The $Q_{xxz}^{(f)}$ component becomes positive again for electrons in CH_4, for the value of E/n_0 where $Q_T^{(f)}$ becomes positive. Thus, it is difficult to find out more about the behaviour of individual

off-diagonal components of the third-order transport tensor, from the presence of NDC in the E/n_0-profile of drift velocity in a given field region, due to the complexity of various factors that determine the behaviour of the third-order transport coefficients. However, it is evident that negative values of $Q_T^{(f)}$ can arise in the vicinity of the field region where NDC occurs. Negative values of $Q_T^{(f)}$ imply the compression of the spatial profile of the swarm along the transverse direction at the front of the swarm, and the expansion of this profile along the same direction at the back of the swarm [57]. This implies that the rapid increase of collision frequency for elastic collisions, which leads to a greater randomization of velocity vectors of the individual electrons and the occurrence of NDC, can also hinder transverse spreading of electrons at the swarm front, where the mean energy of electrons is higher than that at the back of the swarm. This is manifested through negative values of $Q_T^{(f)}$. However, this does not lead to negative values of $Q_L^{(f)}$, as they occur only when the spatial profile of the swarm is skewed in the direction opposite to the direction of drift velocity. This kind of deformation requires a strong resistance to the motion of electrons in the direction of drift velocity, which is more easily achieved with inelastic and non-conservative collisions, when the corresponding cross sections are large enough. It can be seen that $Q_T^{(f)}$ is negative in the majority of region where $Q_L^{(f)}$ is negative for electrons in CF_4, as it is easier to achieve negative values of $Q_T^{(f)}$ than negative values of $Q_L^{(f)}$. Thus, one may conclude that the concurrence between drift velocity and $Q_T^{(f)}$ can be attributed to the corresponding collisions which lead to the occurrence of NDC and to the compression of the spatial distribution of the swarm along the transverse direction at the front of the swarm. However, we observe that for the electrons in CF_4 negative values of $Q_T^{(f)}$ occur only in a small field range after the NDC. Therefore, the presence of NDC at a certain value of E/n_0 does not necessarily result in a negative value of $Q_T^{(f)}$ for these electric fields, but again the conditions in the momentum and energy balances that lead to NDC also favour negative values of Q_T depending on the balance of different competing processes. The concurrence between the transport coefficients of the third-order and the drift velocity is therefore much less pronounced than the concurrence between the transport coefficients of the third-order and diffusion. It would be interesting to investigate the behaviour of $Q_T^{(f)}$ and $Q_T^{(b)}$ in strongly attaching gases under conditions in which NDC occurs only for bulk drift velocity, due to electron attachment [87, 88]. This will be considered in the near future.

It is striking that although similar in the shape of the cross sections the two gases exhibit very different dependences of the NDC. For CF_4 the NDC minimum is much shallower and occurs at higher E/n_0. The depth of the NDC is normally promoted by the separate control of the mean energy and momentum transfer by cross sections that control the energy exchange and momentum transfer. Positioning of vibrational excitation cross sections and overlap of their influences will at the same time affect the magnitude of the peak in drift velocity induced by the inelastic processes and also the onset and overall effect of the NDC.

In figures 5 and 6, we show comparison between the two-term and converged multi-term solutions of the Boltzmann equation for electrons in N_2 and CF_4, respectively. The

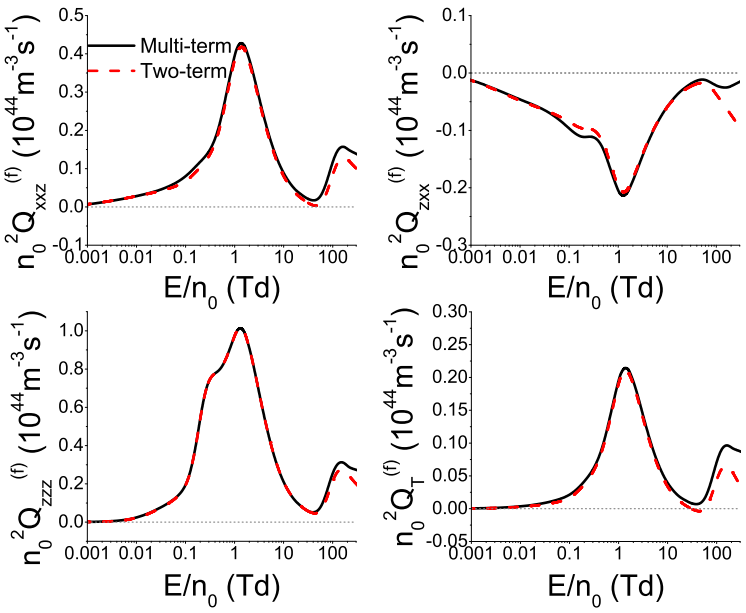

Figure 5. Comparison between the flux third-order transport coefficients obtained by the two-term approximation and multi-term theory for solving the Boltzmann equation. Calculations are performed for electrons in N_2.

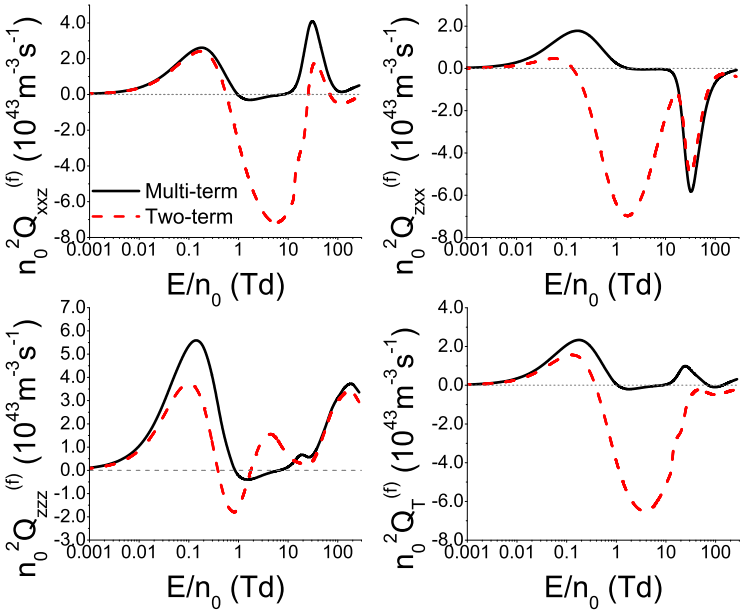

Figure 6. Comparison between the flux third-order transport coefficients obtained by the two-term approximation and multi-term theory for solving the Boltzmann equation. Calculations are performed for electrons in CF_4.

E/n_0 profiles of the independent components of the flux third-order transport tensor, including $n_0^2 Q_{xxz}^{(f)}$, $n_0^2 Q_{zxx}^{(f)}$ and $n_0^2 Q_{zzz}^{(f)}$ are shown. In addition, the variation of $n_0^2 Q_T^{(f)}$ with E/n_0 is also shown. Comparing two-term and multi-term results for electrons in N_2, it is evident that for the low values of E/n_0 the agreement is good while the maximum error in the two-term approximation occurs at the highest fields. For electrons in CF_4, however, there is a significant difference between the two-term and multi-term solutions of the Boltzmann equation over the entire range of E/n_0 considered in this work, except in the limit of the lowest E/n_0. In contrast to N_2, the two-term and multi-term results are qualitatively different in CF_4, indicating that sometimes the two-term theory predicts physics that is not entirely correct. The maximum errors of the two-term approximation occur over the range of E/n_0 values where $n_0^2 Q_{zzz}^{(f)}$ is negative. This happens at electron energies where elastic momentum transfer is approximately at a minimum while inelastic collisions which lead to the vibrational excitations of CF_4 molecule became significant and are approximately at their maximum. This induces a large asymmetry of the distribution function in velocity space which makes the two-term approximation inadequate for studying the third-order transport coefficients. Thus, it is important to note that neglecting higher terms in the spherical harmonic expansion of the phase space distribution function has a much more pronounced effect for third order transport coefficients than for lower order transport coefficients. For electrons in CF_4 the third-order transport coefficients determined by using the two-term approximation are not even qualitatively correct.

4.3. The influence of non-conservative processes on the third-order transport coefficients

4.3.1. The influence of electron attachment on the third-order transport coefficients for electrons in the modified Ness-Robson model The bulk and flux values of the longitudinal and transverse components of the third-order transport tensor for electrons in the Ness-Robson attachment heating model, are shown in figures 7 (a) and (b), respectively. In this model the slower electrons at the back of the swarm are preferentially attached. As a consequence, the bulk values of Q_L and Q_T exceed the corresponding flux values for lower values of E/n_0, e.g., up to about 3.8 Td for Q_L and 5 Td for Q_T.

For higher values of E/n_0, up to about 8 Td for Q_L and 17 Td for Q_T, the flux values are greater than the corresponding bulk values, although this effect is in the limit of statistical error of Monte Carlo simulations in the case of Q_T. This can be attributed to a combination of two factors. The first factor is the decreased number of low-energy electrons at the back of the swarm, due to the rise of the mean energy with increasing field. The second factor is the increased number of low-energy electrons at the front of the swarm, due to the influence of inelastic collisions, which are more frequent at the front of the swarm. In the limit of the highest fields, higher than 8 Td for Q_L and 17 Td for Q_T, the difference between flux and bulk values of the third-order transport

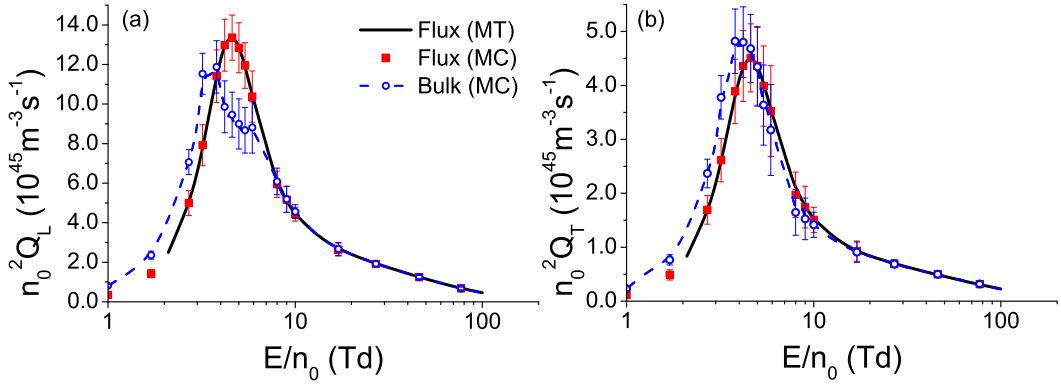

Figure 7. Comparison of the bulk and flux values of (a) $n_0^2Q_L$ and (b) $n_0^2Q_T$ for electrons in the modified Ness-Robson attachment heating model. The results are obtained from numerical multi-term solutions of the Boltzmann equation (MT) and Monte Carlo simulations (MC).

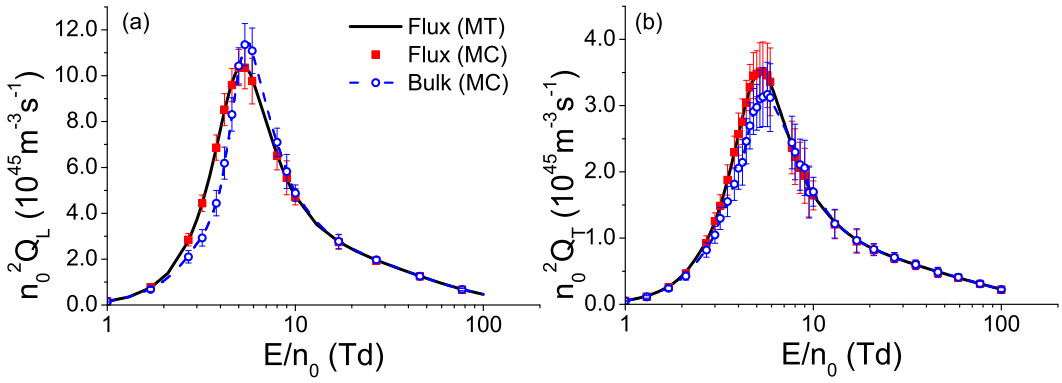

Figure 8. Comparison of the bulk and flux values of (a) $n_0^2Q_L$ and (b) $n_0^2Q_T$ for electrons in the modified Ness-Robson attachment cooling model. The results are obtained from numerical multi-term solutions of the Boltzmann equation (MT) and Monte Carlo simulations (MC).

coefficients is negligible for electrons in this model gas.

The bulk and flux values of the longitudinal and transverse components of the third-order transport tensor for electrons in the Ness-Robson attachment cooling model, are shown in figures 8 (a) and (b), respectively. In this model the faster electrons at the front of the swarm, where the mean energy is higher, are preferentially attached. As a consequence, for lower values of E/n_0 bulk values are lower than the corresponding flux values. We observe that this effect is within the statistical uncertainty of Monte Carlo simulations for Q_T. However, for higher values of E/n_0 (from approximately 5 Td) bulk values are larger than the corresponding flux values in case of Q_L, although this difference is lower than the statistical error of Monte Carlo simulations. For $E/n_0 \geq 10$ Td $Q_L^{(f)}$ and $Q_L^{(b)}$ are practically equal. Similar behaviour is observed for Q_T, because for $E/n_0 \geq 7$ Td $Q_T^{(f)}$ and $Q_T^{(b)}$ coincide. Between 5 Td and 10 Td, $Q_L^{(b)}$ exceeds $Q_L^{(f)}$ due to the interplay of inelastic collisions and the increase of the mean electron energy

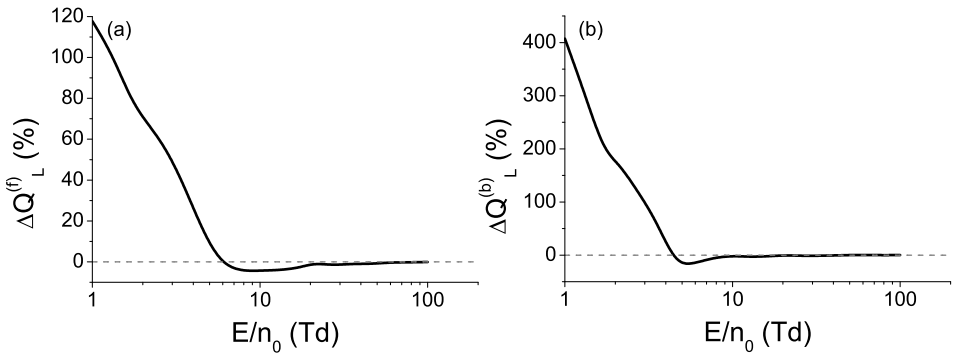

Figure 9. Percentage differences between the values of (a) $Q_L^{(f)}$ and (b) $Q_L^{(b)}$ for electrons in two different versions of the modified Ness-Robson model. Calculations are performed by the Monte Carlo method in the modified Ness-Robson attachment heating model and in the modified Ness-Robson model with a constant collision frequency for electron attachment.

with increasing E/n_0, as in the case of the attachment heating model.

In figure 9 the percentage difference in the longitudinal component of the third-order transport tensor calculated using the modified Ness-Robson models with the attachment heating and with a constant collision frequency for electron attachment, are shown. Panel (a) shows the difference between the flux values, while the panel (b) displays the difference between the bulk values. The percentage differences are calculated using the expression: $Q_L^{heating}/Q_L^{constant} - 1$. The difference between flux values of Q_L in these two models is caused by the implicit effects of electron attachment, while the difference between the corresponding bulk values is induced by a combined effect of implicit and explicit effects of electron attachment. Comparing panels (a) and (b) in the limit of the lowest E/n_0, we observe that Q_L is much higher in the attachment heating model than in the model with a constant collision frequency for electron attachment, for both bulk and flux values. It is also evident that these differences are much more pronounced in the case of bulk third-order transport coefficients. These differences decrease with increasing E/n_0 and become even negative over a limited range of E/n_0. As E/n_0 further increases, the differences tend to zero. It should be noted that negative values of these quantities can be attributed to the influence of inelastic collisions, although these values are within the statistical uncertainty of Monte Carlo simulations.

Similarly, figure 10 shows the difference in Q_L calculated using the modified Ness-Robson models with the attachment cooling and with a constant collision frequency for electron attachment. Results for $Q_L^{(f)}$ and $Q_L^{(b)}$ are shown in panel (a) and panel (b), respectively. In this case, the following expression is used for calculating the percentage difference: $Q_L^{cooling}/Q_L^{constant} - 1$. The values of this expression for the longitudinal components of both flux and bulk third-order transport tensor are decreasing functions of E/n_0 up to about 4 Td where they reach a local minimum, which is equal to around -20% and about -50% for $Q_L^{(f)}$ and $Q_L^{(b)}$, respectively. For higher values of E/n_0 these differences are being increased and they reach a local maximum at around 10 Td in

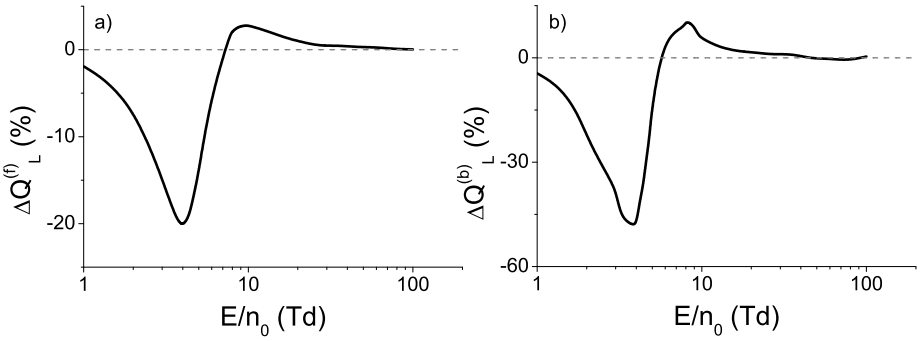

Figure 10. Percentage differences between the values of (a) $Q_L^{(f)}$ and (b) $Q_L^{(b)}$ for electrons in two different versions of the modified Ness-Robson model. Calculations are performed by the Monte Carlo method in the modified Ness-Robson attachment cooling model and in the modified Ness-Robson model with a constant collision frequency for electron attachment.

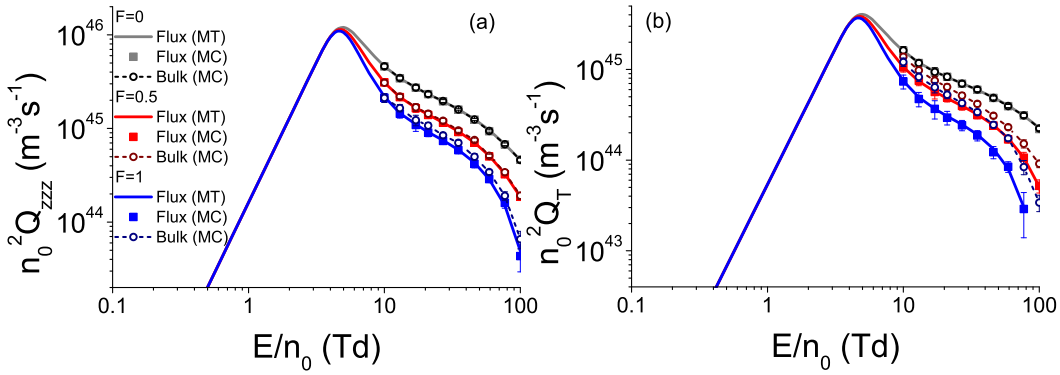

Figure 11. Comparison of the bulk and flux values of (a) $n_0^2 Q_{zzz}$ and (b) $n_0^2 Q_T$ for electrons in the ionisation model of Lucas and Saelee. The results are obtained from numerical multi-term solutions of the Boltzmann equation (MT) and Monte Carlo simulations (MC).

the case of $Q_L^{(f)}$ and at about 8 Td in the case of $Q_L^{(b)}$. This local maximum has a positive value, although this value is within the statistical uncertainty of Monte Carlo simulations. As E/n_0 further increases, these differences converge to zero.

4.3.2. The influence of ionisation on the third-order transport coefficients for electrons in Lucas-Saelee model, N_2 and CF_4 The variation of the flux and bulk Q_L with E/n_0 of electrons in the Lucas-Saelee model for three values of the parameter F is displayed in figure 11 (a). Likewise, figure 11 (b) shows the flux and bulk Q_T as a function of E/n_0. We observe that bulk values are larger than the corresponding flux values for $F = 0.5$ and $F = 1$, due to explicit effects of ionisation on the third-order transport coefficients. Comparing Q_L and Q_T, we see that the difference between bulk and flux values in this model is much higher for Q_T. This can be attributed to strong inelastic and non-conservative collisions that provide strong resistance to the spread of the swarm in the direction of the drift velocity. This significantly inhibits the elongation of the spatial

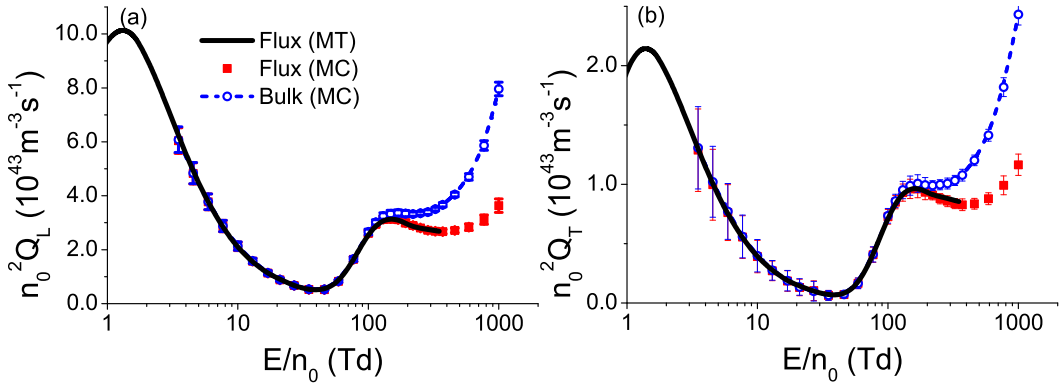

Figure 12. Comparison of the bulk and flux values of (a) $n_0^2Q_L$ and (b) $n_0^2Q_T$ for electrons in N_2. The results are obtained from numerical multi-term solutions of the Boltzmann equation (MT) and Monte Carlo simulations (MC).

distribution of the swarm in the longitudinal direction under the influence of ionisation.

We observe from figure 11 that the flux values of Q_L and Q_T are reduced with increasing parameter F due to ionisation cooling of the swarm. This illustrates the implicit effects of ionisation on the third-order transport coefficients. We also note that bulk values of Q_L and Q_T are being reduced with increasing F. This indicates that the influence of the implicit effects of ionisation on the third-order transport tensor is stronger than the corresponding influence of the explicit effects.

Figures 12 (a) and (b) display the differences between flux and bulk values of Q_L and Q_T respectively, for electrons in N_2. The differences between the flux and bulk values of Q_L and Q_T for electrons in CF_4 are shown in figures 13 (a) and (b), respectively. We observe that bulk values of Q_L and Q_T are larger than the corresponding flux values in both gasses at high electric fields, where electrons undergo many ionisation collisions. Comparing N_2 and CF_4 on one side, and the Lucas-Saelee ionisation model on the other side, we observe that the impact of the explicit effects on the longitudinal component of the third-order transport tensor is much stronger for real gases. This follows from the fact that the minimal impact of the explicit effects of ionisation on Q_L for electrons in the ionisation model of Lucas and Saelee can be attributed to the specific energy dependence of cross sections for inelastic collisions and ionisation. Generally speaking, the qualitative behaviour of the third-order transport coefficients with increasing E/n_0 is the same in the case of flux and bulk values. However, for electrons in N_2, we observe that the bulk values of Q_L and Q_T reach their last local minimum at the lower E/n_0 than the corresponding flux values. Specifically, $Q_L^{(b)}$ and $Q_T^{(b)}$ reach their last local minimum at about 220 Td, while $Q_L^{(f)}$ and $Q_T^{(f)}$ reach their last local minimum at around 370 Td. We also observe from figures 12 and 13 that the results evaluated by multi term solution to the Boltzmann equation and those obtained in Monte Carlo simulations agree very well.

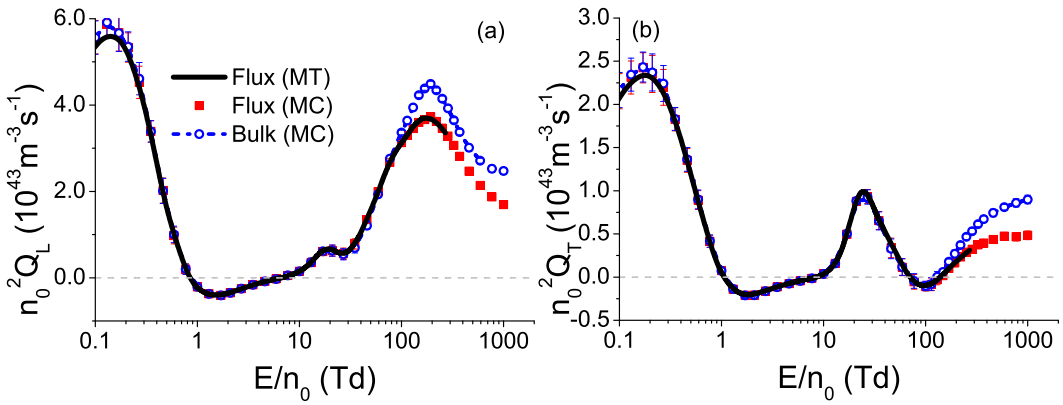

Figure 13. Comparison of the bulk and flux values of (a) $n_0^2Q_L$ and (b) $n_0^2Q_T$ for electrons in CF_4. The results are obtained from numerical multi-term solutions of the Boltzmann equation (MT) and Monte Carlo simulations (MC).

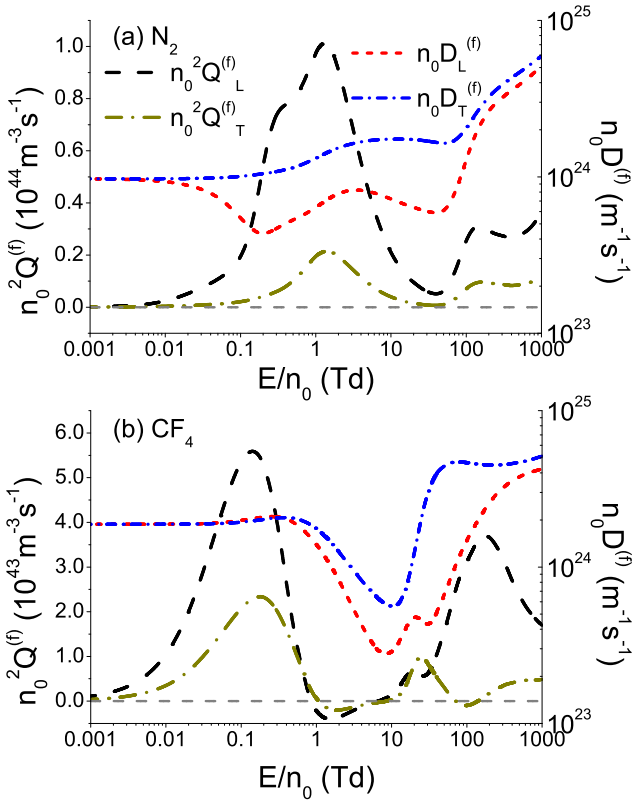

Figure 14. Concurrence of the third-order transport coefficients and diffusion coefficients for electrons in (a) N_2 and (b) CF_4. For $E/n_0 \leq 300$ Td, the results are calculated from numerical multi-term solutions of the Boltzmann equation, while for $E/n_0 > 300$ Td the results are obtained from Monte Carlo simulations.

4.4. Concurrence of the third-order transport coefficients and diffusion, the contribution of $Q_L^{(b)}$ to the spatial profile of the swarm and the comparison of $Q_L^{(b)}$ values obtained in this work with results of previous authors

The concurrence between third-order transport coefficients and diffusion coefficients for electrons in N_2 and CF_4 is illustrated by figures 14 (a) and (b). Preliminary results in

the study of this concurrence for electrons in CH_4 and noble gases have already been discussed [61, 68].

Specifically, for higher values of E/n_0 we observe that $Q_L^{(f)}$ is a rising function of E/n_0 when $D_L^{(f)}$ increases as a convex (or linear) function of E/n_0 in the log-log scale. One may also observe that $Q_L^{(f)}$ is reduced when $D_L^{(f)}$ decreases, or when $D_L^{(f)}$ rises as a concave function of the field in the log-log scale. This concurrence is absent in the limit of the lowest E/n_0 because the third-order transport coefficients vanish in this range of fields unlike diffusion coefficients which have non-zero thermal values.

As can be seen in figure 14 (a) the concurrence between $Q_L^{(f)}$ and $D_L^{(f)}$ for electrons in N_2 is present in the entire field region above 0.21 Td. For electrons in CF_4, we observe that the concurrence between $Q_L^{(f)}$ and $D_L^{(f)}$ is present in the subset of the field range above 0.02 Td, where $Q_L^{(f)}$ is positive (see figure 14 (b)). However, this concurrence is absent in the field range between 1.6 Td and 8.5 Td, as $Q_L^{(f)}$ rises with increasing E/n_0 although $D_L^{(f)}$ is being reduced in this field range. It is important to note that $Q_L^{(f)}$ has negative values over the range of E/n_0 in this field region. Further increase of the absolute value of $Q_L^{(f)}$, while this component is negative, would imply a further skewing of the spatial profile of the swarm in the negative direction (opposite to the drift velocity) along the longitudinal axis. Although the rise of the collision frequency for vibrational excitations with increasing E/n_0 is strong enough to cause a decrease of $D_L^{(f)}$, it is not strong enough to induce further skewing of the spatial profile of the swarm in the negative direction. It is interesting to note that the concurrence between $Q_L^{(f)}$ and $D_L^{(f)}$ is again present at about 8.5 Td, which is slightly above the field where $Q_L^{(f)}$ becomes positive again (at around 7 Td).

For electrons in N_2, the qualitative trends of $D_L^{(f)}$ and $D_T^{(f)}$ are the same in the field range above 0.21 Td, where the concurrence between $Q_L^{(f)}$ and $D_L^{(f)}$ is clearly evident. Thus, it is difficult to determine if the E/n_0 profile of $Q_T^{(f)}$ is more related to the corresponding profile of $D_L^{(f)}$ or $D_T^{(f)}$ in the case of N_2. For electrons in CF_4, E/n_0 profile of $Q_T^{(f)}$ is related to the corresponding profile of $D_T^{(f)}$ in most of the field range where $Q_T^{(f)}$ is positive. The concurrence between these two transport coefficients in CF_4 is equivalent to the concurrence between $Q_L^{(f)}$ and $D_L^{(f)}$, which is already discussed in this paper. This concurrence is absent in the field region between approximately 100 Td and 170 Td. However, $Q_T^{(f)}$ is negative up to around 140 Td. Thus, the field dependence of $Q_T^{(f)}$ is not related to the field dependence of diffusion in the field range where it is negative, and in the vicinity of the field where it becomes positive, similarly to $Q_L^{(f)}$.

The physical reasons for the observed concurrence between the third-order transport coefficients and diffusion coefficients have been discussed in our previous paper [68] for the example of atomic gases with considerably simpler sets of cross sections. The third-order transport coefficients represent a small asymmetric correction to diffusive motion, that is represented by the components of the diffusion tensor. As discussed previously [57], the rise of the reduced electric field leads to an increase of the directional component of electron velocity (in the absence of NDC) and to an increase of the electron energy. These two effects favor the increase of the third-order transport coefficients if

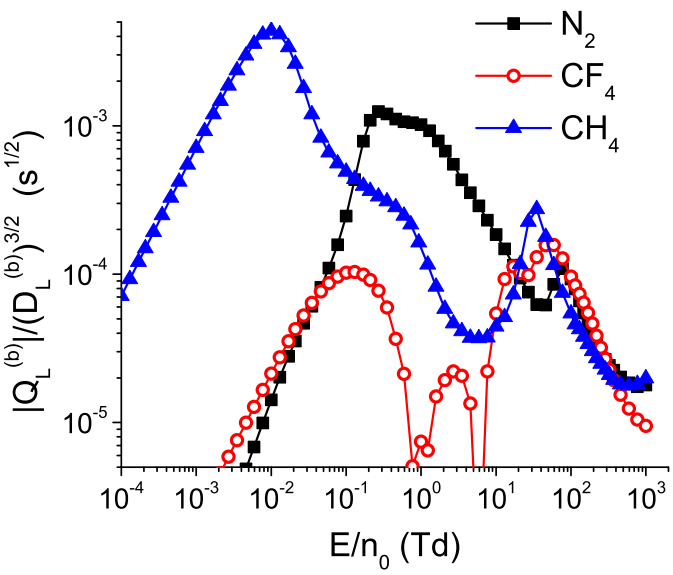

Figure 15. The values of the ratio $|Q_L^{(b)}|/(D_L^{(b)})^{3/2}$ for electrons in N_2, CF_4 and CH_4 as functions of E/n_0. For $E/n_0 \leq 100$ Td, where the differences between the bulk and flux values are negligible, the results are obtained from numerical multi-term solutions of the Boltzmann equation, while for higher values of E/n_0 the results are obtained in Monte Carlo simulations.

the frequency of electron collisions with atoms/molecules of the background gas is not rising with increasing energy. However, if the collision frequency is rising steeply enough with increasing electron energy, this leads to a reduction of the third-order transport coefficients. The same holds for the components of the diffusion tensor, which are also quenched by elastic and inelastic collisions. Comparing these two sets of transport coefficients, third-order transport coefficients represent a form of motion that 'carries' a smaller amount of energy and momentum, and as such they are much more sensitive to collisions with the background gas, than the components of the diffusion tensor. This suggests that for a sufficiently high E/n_0, the third-order transport coefficients are reduced with increasing E/n_0, if the diffusion is being reduced, and even if the slope of diffusion in the log-log scale decreases with increasing E/n_0. However, this concurrence is absent at the lowest fields and under conditions in which third-order transport coefficients are negative, due to reasons that are already discussed in this manuscript.

In figure 15 we show the values of the ratio $|Q_L^{(b)}|/(D_L^{(b)})^{3/2}$ for electrons in N_2, CF_4 and CH_4, as functions of E/n_0. Calculations are performed assuming the concentration of background molecules $n_0 = 3.54 \cdot 10^{22}$ m^{-3}. This ratio determines the contribution of the longitudinal component of the third-order transport tensor to the spatial profile of the swarm, as can be seen from equation (6). From this figure, we observe that the contribution of $Q_L^{(b)}$ to the spatial profile of the swarm is larger in CH_4 than in the remaining two gases for E/n_0 lower than 0.1 Td and for E/n_0 between 21 Td and 46 Td. For E/n_0 between 0.13 Td and 17 Td the quantity $|Q_L^{(b)}|/(D_L^{(b)})^{3/2}$ is larger in N_2

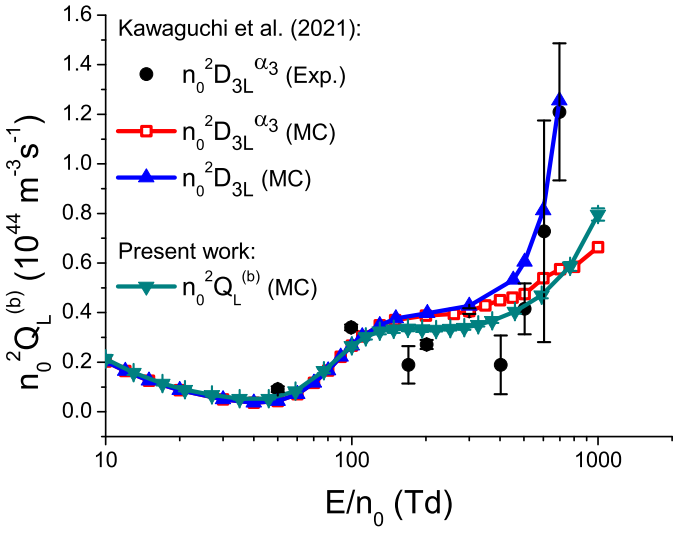

Figure 16. Comparison of the values of $n_0^2 Q_L^{(b)}$, that are determined in this work, with the results of Kawaguchi *et al.* [58]. In this figure $n_0^2 D_{3L}$ represents simulation results from the reference [58] that are determined from equation (24) by employing Monte Carlo simulations, while $n_0^2 D_{3L}^{\alpha_3}$ represents $n_0^2 Q_L^{(b)}$ that are determined in reference [58] form alpha parameters, after neglecting alpha paramethers of fourth and higher order. Experimental results of Kawaguchi *et al.* are represented by black circles, while results that are obtained from Monte Carlo simulations are represented by a combination of symbols and continuous lines.

than in CH_4 and CF_4. For E/n_0 between 70 Td and 300 Td this ratio is slightly lower in CH_4 than in the remaining two gases. For E/n_0 between 400 Td and 1000 Td this ratio is lower in CF_4 than in N_2 and CH_4. It is interesting to note that differences between the values of $|Q_L^{(b)}|/(D_L^{(b)})^{3/2}$ in N_2, CH_4 and CF_4 do not exceed the factor of three in the field range between 50 Td and 700 Td. In most of this region, these differences do not exceed the factor of two. Moreover, the values of this ratio are very close to each other for electrons in these three gases in the field range between 200 Td and 450 Td. This indicates that $n_0^2 Q_L^{(b)}$ can be measured in CH_4 and CF_4, in the field range between 50 Td and 700 Td, under similar experimental conditions that were applied for measurements in N_2. Recently Kawaguchi and coworkers using a Monte Carlo simulation technique have shown that $n_0^2 Q_L^{(b)}$ can be measured in CH_4 and SF_6 in the arrival time spectra experiment [70].

In figure 16 we show the comparison of the longitudinal component of the third-order transport tensor $n_0^2 Q_L^{(b)}$ for electrons in N_2 with the corresponding values that are determined by Kawaguchi *et al.* [58]. In this figure, $n_0^2 D_{3L}$ is determined from Monte Carlo simulations by using equation (24), while $n_0^2 D_{3L}^{\alpha_3}$ is evaluated from the alpha parameters based on equation (25) from reference [58] by neglecting the alpha parameters of fourth and higher order. Kawaguchi and coworkers determined alpha parameters from the arrival time spectra experiment and the Monte Carlo simulations. All results are in an excellent agreement up to about 130 Td, while differences between

these sets of results become noticeable at higher values of E/n_0. Our calculated values of $n_0^2 Q_L^{(b)}$ are somewhat lower than the theoretical results of Kawaguchi *et al.* for E/n_0 between 130 Td and 460 Td. For higher values of E/n_0 our results are significantly lower than $n_0^2 D_{3L}$ and somewhat below $n_0^2 D_{3L}^{\alpha_3}$ until approximately 770 Td. At around 1000 Td the value of $n_0^2 Q_L^{(b)}$ in the present calculations, is somewhat above the theoretical values of $n_0^2 D_{3L}^{\alpha_3}$ that are determined by Kawaguchi *et al.* The difference between our calculations of $n_0^2 Q_L^{(b)}$ and those of Kawaguchi and co-workers for $n_0^2 D_{3L}$ is a clear indication of different sets of cross sections used as input data in Monte Carlo simulations. The sensitivity of the third-order transport coefficients to the cross sections used in the transport calculations was demonstrated by Kawaguchi and coworkers [62]. The deviation of $n_0^2 D_{3L}^{\alpha_3}$ from $n_0^2 D_{3L}$ for higher values of E/n_0 can be attributed to neglecting alpha parameters of fourth and higher order in equation from which the values of $n_0^2 D_{3L}^{\alpha_3}$ are determined, as discussed by Kawaguchi *et al.* [58]. Our calculations of $n_0^2 Q_L^{(b)}$ and experimental values of $n_0^2 D_{3L}^{\alpha_3}$ agree very well up to about 600 Td. If we take a careful look, we observe that our calculations are somewhat below experimental values up to about 100 Td and somewhat above experimental results until approximately 500 Td. For higher values of E/n_0, however, our results are significantly below experimental points. For $E/n_0 = 600$ Td our calculations of $n_0^2 Q_L^{(b)}$ are within the experimental error, while at 700 Td they are significantly below the lower boundary of experimental results at 700 Td. Strictly speaking, $n_0^2 Q_L^{(b)}$ and $n_0^2 D_{3L}^{\alpha_3}$ cannot be directly equated, because $n_0^2 D_{3L}^{\alpha_3}$ represents an approximation of $n_0^2 Q_L^{(b)}$ when the fourth and higher order alpha parameters are negligible. Strict comparison with experimental results obtained by Kawaguchi and coworkers [58] would be possible if $n_0^2 D_{3L}^{\alpha_3}$ was determined using measured or calculated alpha parameters.

5. Conclusion

In this paper, we have investigated the behaviour of the third-order transport coefficients for electrons in N_2 and CF_4. Calculations have been performed using a multi-term theory for solving the Boltzmann equation and Monte Carlo simulation technique. The initial Monte Carlo code has been extended to allow the calculations of third-order transport coefficients in the presence of non-conservative collisions. We found that the moment method for solving the Boltzmann equation works very well for the third-order transport coefficients, and is particularly fast and accurate for model gases.

One of the most striking phenomena observed in the present work is the occurrence of negative values in the E/n_0-profiles of $n_0^2 Q_{xxz}^{(f)}$ and $n_0^2 Q_{zzz}^{(f)}$ for electrons in CF_4. After the relaxation of the swarm to the steady-state, transport coefficients of the third-order attain negative values over the range of electron energies where the most energetic electrons may undergo many collisions leading to the vibrational excitation of CF_4 molecule. We have also noticed that the occurrence of negative values in the E/n_0-profiles of $n_0^2 Q_{xxz}^{(f)}$ and $n_0^2 Q_{zzz}^{(f)}$ in CF_4 takes place in the energy region where the cross sections for vibrational excitations exceed the cross section for momentum transfer in

elastic collisions. Likewise, we have also observed that $n_0^2 Q_T^{(f)}$ has negative values in the field region between the end of the occurrence of NDC and the field where the drift velocity reaches 90% of its initial value before the onset of NDC. Based on the results presented in this work, it may be assumed that there is a slight concurrence between $n_0^2 Q_T^{(f)}$ and drift velocity. This concurrence refers to the occurrence of negative values of $n_0^2 Q_T^{(f)}$ that are essentially controlled by the collision processes, which promote the development of NDC.

As the two-term approximation has become a commonplace in the calculation of electron transport properties in gases and as it forms the foundations of many publicly available codes for solving the Boltzmann equations, we have been motivated to investigate its limitations in the context of the present research. Comparisons between the two-term and multi-term calculations were performed for E/n_0 less than 300 Td. For electrons in N_2, the accuracy of the two-term approximation is sufficient to investigate the behaviour of the third-order transport coefficients in the presence of the electric field. In contrast, for electrons in CF_4 the two-term approximation produces large errors and it is not even qualitatively correct, particularly over the range of electron energies where the cross section for transfer of momentum in elastic collisions is at minimum, while the cross sections of vibrational excitations become significant. This favours a large asymmetry in the distribution function in the velocity space which in turn renders the two-term approximation quite inappropriate for the analysis of third-order transport coefficients.

In the present work, we have studied the implicit and explicit effects of non-conservative collisions on the third-order transport coefficients. While implicit effects of non-conservative collisions are induced by direct population and depopulation of the distribution function in velocity space, the explicit effects are caused by the combined effects of the energy dependence of non-conservative collisions and spatial variation of the average energy along the swarm. Using the modified Ness-Robson model with the attachment heating, we have observed that the bulk values of $n_0^2 Q_L$ and $n_0^2 Q_T$ are larger than the corresponding flux values at low electric fields. At intermediate fields the opposite situation holds: the flux values are larger than the corresponding bulk values. This behaviour and relationship between the bulk and flux values of both $n_0^2 Q_L$ and $n_0^2 Q_T$, are inverted for the attachment cooling model.

The effects of electron-impact ionisation on the third-order transport coefficients are analysed for electrons in the ionisation model of Lucas and Saelee, N_2 and CF_4. For all gases we considered, bulk values of $n_0^2 Q_L$ and $n_0^2 Q_T$ are larger than the corresponding flux values for the higher electric fields. In particular, comparing the explicit influence of ionisation on $n_0^2 Q_L^{(b)}$ and $n_0^2 Q_T^{(b)}$ in the ionisation model of Lucas and Saelee, effects are more pronounced for $n_0^2 Q_T^{(b)}$.

In this work the concurrence between $n_0^2 Q_L^{(f)}$ and $n_0 D_L^{(f)}$ is analysed. For electrons in N_2 the concurrence is effective over the entire range of the considered E/n_0. This concurrence is also present for electrons in CF_4 over the range of E/n_0 where $n_0^2 Q_L^{(f)}$ is positive. However, in the field region where $n_0^2 Q_L^{(f)}$ is negative, there is a range of E/n_0

values, where $n_0^2 Q_L^{(f)}$ is rising although $n_0 D_L^{(f)}$ is being reduced. This effect is analysed using the physical interpretation of the negative values of $n_0^2 Q_L^{(f)}$. The concurrence between $n_0^2 Q_T^{(f)}$ and the components of the diffusion tensor is also investigated. In particular, for electrons in CF_4 we found that the E/n_0 profile of $n_0^2 Q_T^{(f)}$ is more related to the corresponding profile of $n_0 D_T^{(f)}$ than to the corresponding profile of $n_0 D_L^{(f)}$.

Contribution of the longitudinal component of the third-order transport tensor to the spatial profile of the swarm was studied for electrons in N_2, CF_4 and CH_4. This contribution is proportional to the ratio $|Q_L^{(b)}|/(D_L^{(b)})^{3/2}$. Between 50 Td to 700 Td differences between the values of this ratio for electrons in N_2, CF_4 and CH_4 do not exceed the factor of 3. More precisely, we have observed that these differences do not differ from each other by a factor of 2 over the majority of E/n_0 values in the above-mentioned field region. Even though this result of the study seems modest, it is very important because it shows that the existing experimental infrastructure used to measure third-order transport coefficients in N_2 can be used equally successfully for measurements of these quantities in other gases.

The present calculations of $n_0^2 Q_L^{(b)}$ for electrons in N_2 are compared with the arrival time spectra measurements and Monte Carlo simulations of Kawaguchi and coworkers [58]. The present calculations and results of Kawaguchi and coworkers agree very well up to approximately 500 Td. For higher values of E/n_0, the discrepancy between our calculations and those obtained by Kawaguchi and coworkers in Monte Carlo simulations, may be directly attributed to the details of the cross sections for electron scattering in N_2 used as input data in numerical codes.

It is hoped that the present study will provide an incentive for further theoretical and experimental studies of the third-order transport coefficients for electrons in gases. Particular attention has recently been focused on extracting cross-sections from swarm data [89, 90]. The inclusion of these sensitive higher order transport coefficients, may result in improved cross-section sets, particularly given the new machine learning algorithms implemented [91–93]. Our plans for future research include the study of third-order transport coefficients in the presence of pressure dependent effects and third-order transport coefficients for positrons in gases of interest for further development and optimization of positron traps.

6. Acknowledgments

The authors acknowledge the support of the Institute of Physics Belgrade and the Ministry of Education, Science and Technological Development of the Republic of Serbia. Z. Lj. Petrović is grateful to the SASA F155 project for support. R.D. White acknowledges the financial support from the Australian Research Council scheme.

References

[1] Lieberman M A and Lichtenberg A J, *Principles of Plasma Discharges and Materials Processing* (Wiley-Interscience, 2005)

[2] Makabe T and Petrović Z Lj, *Plasma Electronics: Applications in Microelectronic Device Fabrication* (New York, CRC Press, 2014)

[3] Rudenko K V 2009 *High Energy Chem.* **43** 196

[4] Shustin E G 2017 *J. Commun. Technol. Electron.4* **62** 454

[5] Shamiryan D, Paraschiv V, and Boullart W 2009 *High Energy Chem.* **43** 204

[6] Donnelly V M and Kornblit A 2013 *J. Vac. Sci. Technol. A* **31** 050825

[7] Shahidi S and Ghoranneviss M 2015 *Cloth. Text. Res. J.* **34** 37

[8] Xie L, Brault P, Bauchire J M, Thomann A L and Bedra L 2014 *J. Phys. D: Appl. Phys.* **47** 224004

[9] Friedrich J F, Wettmarshausen S, Hanelt S, Mach R, Mix R, Zeynalov E B, and Meyer-Plath A 2010 *Carbon* **48** 3884

[10] Takai O 2008 *Pure Appl. Chem.* **80** 2003

[11] Weltmann K D and von Woedtke Th 2017 *Plasma Phys. Control. Fusion* **59** 014031

[12] Laroussi M 2018 *Plasma* **1** 47

[13] Griseti E, Kolosnjaj-Tabi J, Gibot L, Fourquaux I, Rols M P, Yousfi M, Merbahi N, and Golzio M 2019 *Sci. Rep.* **9** 7583

[14] Alves L L, Bogaerts A, Guerra V and Turner M M 2018 *Plasma Sources Sci. Technol.* **27** 023002

[15] Colonna, G., Pintassilgo C.D., Pegoraro F., Cristofolini A., Popoli A., Neretti G., Gicquel A., Duigou O., Bieber T., Hassouni K. and Laguardia L. 2021 *Eur. Phys. J. D* **75** 183

[16] Makabe T 2018 *Plasma Sources Sci. Technol.* **27** 033001

[17] Madshaven I, Hestad O L, and Åstrand P-O 2021 *Comput. Phys. Commun.* **265** 107987

[18] Petrović Z Lj, Dujko S, Marić D, Malović G, Nikitović Ž, Šašić O, Jovanović J, Stojanović V and Radmilović-Radjenović 2009 *J. Phys. D: Appl. Phys.* **42** 194002

[19] Ruiz-Vargas G, Yousfi M and de Urquijo J 2010 *J. Phys. D: Appl. Phys.* **43** 455201

[20] Makabe T 2019 *Jpn. J. Appl. Phys.* **58** 110101

[21] Silva T, Grofulović M, Klarenaar B L M, Morillo-Candas A S, Guaitella O, Engeln R, Pintassilgo C D and Guerra V 2018 *Plasma Sources Sci. Technol.* **27** 015019

[22] Minesi N, Mariotto P, Pannier E, Stancu G D and Laux C O 2021 *Plasma Sources Sci. Technol.* **30** 035008

[23] Ribière M, Eichwald O, and Yousfi M 2020 *J. Appl. Phys.* **128** 093304

[24] Upadhyay R R, Suzuki K, Raja L L , Ventzek P L G and Ranjan A 2020 *J. Phys. D: Appl. Phys.* **53** 435209

[25] Nijdam S, Teunissen J, and Ebert U 2020 *Plasma Sources Sci. Technol.* **29** 103001

[26] Arslanbekov R R and Kolobov V I 2021 *Plasma Sources Sci. Technol.* **30** 045013

[27] Marinov D, Teixeira C and Guerra V 2017 *Plasma Process. Polym.* **14** 1600175

[28] Derzsi A, Horvath B, Donko Z and Schulze J 2020 *Plasma Sources Sci. Technol.* **29** 074001

[29] Huxley L G H. and Crompton R W, *The Diffusion and Drift of Electrons in Gases* (Wiley, London, 1974)

[30] Dyatko N A, Kochetov I V, and Ochkin V N 2020 *Plasma Sources Sci. Technol.* **29** 125007

[31] Babaeva N Yu and Naidis G V 2016 *Phys. Plasmas* **23** 083527

[32] Babaeva N Yu and Naidis G V 2018 *Plasma Sources Sci. Technol.* **27** 075018

[33] Li X, Sun A, Zhang G and Teunissen J 2020 *Plasma Sources Sci. Technol.* **29** 065004

[34] Bagheri B, Teunissen J, Ebert U, Becker M M, Chen S, Ducasse O, Eichwald O, Loffhagen D, Luque A, Mihailova D, Plewa J M, van Dijk J and Yousfi M 2018 *Plasma Sources Sci. Technol.* **27** 095002

[35] Arcese E, Rogier F and Boeuf J P 2017 *Physics of Plasmas* **24** 113517

[36] Dujko S, Markosyan A H, White R D and Ebert U 2013 *J. Phys. D: Appl. Phys.* **46** 475202

[37] Taran M D, Dyatko N A, Kochetov I V, Napartovich A P, and Akishev Yu S 2018 *Plasma Sources Sci. Technol.* **27** 055004
[38] Peng Y, Chen X, Lan L, Zhan H, Liu Y, He W, and Wen X 2021 *Plasma Sci. Technol.* **23** 064013
[39] Petrović Z Lj, Šuvakov M, Nikitović Ž, Dujko S, Šašić O, Jovanović J, Malović G and Stojanović V 2007 *Plasma Sources Sci. Technol.* **16** S1-S12
[40] Pitchford L C, Alves L L, Bartschat K, Biagi S F , Bordage M C, Phelps A V, Ferreira C M, Hagelaar G J M, Morgan W L, Pancheshnyi S, Puech V, Stauffer A and Zatsarinny O 2013 *J. Phys. D: Appl. Phys.* **46** 334001
[41] Rabie M, Haefliger P, Chachereau A and Franck C M 2015 *J. Phys. D: Appl. Phys.* **48** 075201
[42] Grofulović M, Alves L L and Guerra V 2016 *J. Phys. D: Appl. Phys.* **49** 395207
[43] Li C, Brok W J M, Ebert U and van der Mullen J J A M 2007 *J. Appl. Phys.* **101** 123305
[44] Chao Li, Teunissen J, Nool M, Hundsdorfer W and Ebert U 2012 *Plasma Sources Sci. Technol.* **21** 055019
[45] Higginson D P, Holod I and Link A 2020 *J. Comput. Phys.* **413** 109450
[46] Wilczek S, Trieschmann J, Eremin D, Brinkmann R P, Schulze J, Schuenge E, Derzsi A, Korolov I, Hartmann P, Donkó Z, and Mussenbrock T 2016 *Phys. Plasmas* **23** 063514
[47] Hartmann P, Wang L, Nösges K, Berger B, Wilczek S, Brinkmann R P, Mussenbrock T, Juhasz Z, Donkó Z, Derzsi A, Lee E, and Schulze J 2020 *Plasma Sources Sci. Technol.* **29** 075014
[48] Takahashi H and Sugawara H 2020 *Jpn. J. Appl. Phys.* **59** 036001
[49] Nakashima K, Takahashi H, and Sugawara H 2019 *Jpn. J. Appl. Phys.* **58** 116001
[50] Pitchford L C *et al.* 2016 *Plasma Process. Polym.* **14** 1600098
[51] Lovaas T H, Skullerud H R, Kristensen 0-H and Linhjell D 1987 *J. Phys. D: Appl. Phys.* **20** 1465
[52] Koutselos A D 2001 *Chem. Phys.* **270** 165
[53] Viehland L A and Johnsen R 2019 *J. Geophys. Res.:Atmospheres* **124** 13,593–13,600
[54] Viehland L A, *Gaseous Ion Mobility, Diffusion, and Reaction* (Springer International Publishing 2018)
[55] Vrhovac S B, Petrović Z Lj, Viehland L A and Santhanam T S 1999 *J. Chem. Phys.* **110** 2423
[56] Sugawara H and Sakai Y 2006 *Jpn. J. Appl. Phys.* **45** 5189
[57] Simonović I, Bošnjaković D, Petrović Z Lj, Stokes P, White R D and Dujko S 2020 *Phys. Rev. E* **101** 023203
[58] Kawaguchi S, Nakata N, Satoh K, Takahashi K and Satoh K 2021 *Plasma Sources Sci. Technol.* **30** 035006
[59] Dujko S, White R D and Petrović Z Lj 2008 *J. Phys. D: Appl. Phys.* **41** 245205
[60] Penetrante B M and Bardsley J N, in *Non-equilibrium Effects in Ion and Electron Transport*, edited by J.W. Gallagher, D.F. Hudson, E.E. Kunhardt, and R.J. Van Brunt (Plenum, New York, 1990), p. 49.
[61] Petrović Z Lj, Simonović I, Marjanović S, Bošnjaković D, Marić D, Malović G and Dujko S 2017 *Plasma Phys. Control. Fusion* **59** 014026
[62] Kawaguchi S, Takahashi K and Satoh K 2021 *Plasma Sources Sci. Technol.* **30** 035010
[63] Stojanović V. D. and Petrović Z. Lj. 1998 *J. Phys. D: Appl. Phys.* **31** 834
[64] Whealton J H and Mason E A 1974 *Ann. Phys.* **84** 8
[65] Koutselos A D 1996 *J. Chem. Phys.* **104** 8442
[66] Koutselos A D 1997 *J. Chem. Phys.* **106** 7117
[67] Koutselos A D 2001 *Chem. Phys.* **315** 193
[68] Simonović I, Bošnjaković D, Petrović Z Lj, White R D and Dujko S 2020 *Eur. Phys. J. D* **74** 63
[69] Stokes P W, Simonović I, Philippa B, Cocks D, Dujko S and White R D 2018 *Sci. Rep.* **8** 2226
[70] Kawaguchi S, Takahashi K and Satoh K 2018 *Plasma Sources Sci. Technol.* **27** 085006
[71] Kumar K, Skullerud H R and Robson R E 1980 *Aust. J. Phys.* **33** 343
[72] Nolan A M, Brennan M J, Ness K F and Wedding A B 1997 *J. Phys. D: Appl. Phys.* **30** 2865
[73] Franceschini C and Loperfido N 2019 *Symmetry* **11** 970
[74] Dujko S, White R D, Petrović Z Lj and Robson R E 2010 *Phys. Rev. E* **81** 046403

[75] Robson R E and Ness K F 1986 *Phys. Rev. A* **33** 2068
[76] White R D, Robson R E, Ness K F and Li B 1999 *Phys. Rev. E* **60** 2231
[77] White R D, Robson R E, Dujko S, Nicoletopoulos P and Li B 2009 *J. Phys. D: Appl. Phys.* **42** 194001
[78] Dujko S, White R D, Petrović Z Lj and Robson R E 2011 *Plasma Sources Sci. Technol.* **20** 024013
[79] Ness K F and Robson R E 1986 *Phys. Rev. A* **34** 2185
[80] Raspopović Z M, Sakadžić S, Bzenić S and Petrović Z Lj 1999 *IEEE Trans. Plasma Sci.* **27** 1241
[81] Petrović Z Lj, Raspopović Z M, Dujko S and Makabe T 2002 *Appl. Surf. Sci.* **192** 1
[82] Dujko S, Raspopović Z M and Petrović Z Lj 2005 *J. Phys. D: Appl. Phys.* **38** 2952
[83] Lucas J and Salee H T 1975 *J. Phys. D: Appl. Phys.* **8** 64
[84] Kurihara M, Petrović Z Lj and Makabe T 2000 *J. Phys. D: Appl. Phys.* **33** 2146
[85] Šašić O, Malović G, Strinić A, Nikitović Ž and Petrović Z Lj 2004 *New J. Phys.* **6** 74
[86] Petrović Z Lj, Crompton R W and Haddad G N 1984 *Aust. J. Phys.* **37** 23
[87] Vrhovac S B and Petrović 1996 *Phys. Rev. E*, **53** 4012
[88] Mirić J, Bošnjaković D, Simonović I, Petrović Z Lj and Dujko S 2016 *Plasma Sources Sci. Technol.* **25** 065010
[89] White R D, Cocks D, Boyle G, Case M, Garland N, Konovalov D, Philippa B, Stokes P, de Urquijo J, González-Magaña O, McEachran R P, Buckman S J, Brunger M J, Garcia G, Dujko S, and Petrović Z L 2018 *Plasma Sources Sci. Technol.* **27** 053001
[90] Casey M J E, de Urquijo J, Serkovic Loli L N, Cocks D G, Boyle G J, Jones D B, Brunger M J, and White R D 2017 *J. Chem. Phys.* **147** 195103
[91] Stokes P W, Cocks D G, Brunger M J, and White R D 2020 *Plasma Sources Sci. Technol.* **29** 055009
[92] Stokes P W, Casey M J E, Cocks D G, de Urquijo J, Garcia G, Brunger M J, and White R D 2020 *Plasma Sources Sci. Technol.* **29** 105008
[93] Stokes P W, Foster S P, Casey M J E , Cocks D G, González-Magaña O, de Urquijo J, García G, Brunger M J, and White R D 2021 *J. Chem. Phys.* **154** 084306